SGG SGS sc | nat
Swiss Journal of Geosciences

RESEARCH

Open Access

Lateglacial to Early Holocene glacier fluctuations in the northern Valaisian Alps

Mattia Binaghi[1*], Naki Akçar[1*], Susan Ivy-Ochs[2,4], Serdar Yeşilyurt[3], Marcus Christl[4] and Christian Schlüchter[1]

Abstract

The northern Valaisian Alps represents a glacially overprinted landscape, characterized by abundant glacial deposits and landforms. Well-preserved moraine systems, commonly found in the region, were deposited by glacier fluctuations after the Last Glacial Maximum (LGM). In this study, we focus on the glacial evolution of the tributary valleys of Belalp and Luesgenalp, west of the Great Aletsch glacier, during the Lateglacial and Early Holocene. To reconstruct the glacier advances, a combination of geomorphological mapping, surface exposure dating with cosmogenic ^{10}Be, and glacier reconstruction were used. Our results indicate that glacier fluctuations occurred at 12.0 ± 0.9 ka in the Belalp valley and 12.0 ± 1.0 ka in the Luesgenalp valley during the Younger Dryas cold phase. Based on the glacier reconstruction, an equilibrium line altitude (ELA) of 2700 m asl was estimated for the maximal extent of these paleoglaciers. ELA depressions of 330 m to 430 m relative to the Little Ice Age for the Unnerbaech paleoglacier in the Belalp valley and 400 m for the Hostock paleoglacier in the Luesgenalp valley were calculated, corresponding to annual temperature decreases of 2.1 to 2.8 °C and 2.6 °C, respectively. The precipitation pattern shows no significant change in the amount of precipitation between YD and today. Our findings are consistent with the YD paleoglaciers documented throughout the Alps and provide insights into the climate dynamics during the Egesen stadial in the Alps. Additionally, our findings contribute to the broader understanding of glacial responses to climatic fluctuations.

Keywords Cosmogenic ^{10}Be, Surface exposure dating, Alps, Glacier reconstruction, Younger Dryas, Paleoclimate

1 Introduction

The last major glacier readvance phase of the Lateglacial occurred during the Younger Dryas cold period (YD), between 12.9 ka and 11.7 ka (Alley and Clark, 1999; Rasmussen et al., 2006; Ivy-Ochs et al., 2023). This cooling event is the final cold phase of the Last Glacial cycle before the transition to the Holocene, during which an abrupt temperature increase is observed (Ivy-Ochs et al., 1996; Ivy-Ochs, 2015; Baroni et al., 2021 and references therein). The YD is a key period for understanding not just the demise of the Last Glacial cycle, but also the remarkable and still poorly understood readvances of glaciers during the Lateglacial, as well as their influence on regional climate from the Last Glacial Maximum (LGM) to the present day (Alley, 2000; Bakke et al., 2009; Rea et al., 2020). Several proxies have recorded this climate fluctuation with a similar magnitude, i.e. ice cores (Rasmussen et al., 2006), lake sediments (Schwander et al., 2000) and speleothems (Affolter et al., 2019). All indicate an abrupt temperature drop at the beginning and a strong temperature increase at the end of the YD (Alley, 2000; Bakke et al., 2009).

Editorial handling: Wilfried Winkler

*Correspondence:
Mattia Binaghi
mattiabinaghi97@gmail.com
Naki Akçar
naki.akcar@unibe.ch
[1] Institute of Geological Sciences, University of Bern, Baltzerstrasse 1+3, CH-3012 Bern, Switzerland
[2] Department of Earth and Planetary Sciences, ETH Zürich, Sonneggstrasse 5, CH-8092 Zurich, Switzerland
[3] Department of Geography, Ankara University, 06230 Ankara, Turkey
[4] Department of Physics, ETH Zürich, Otto-Stern-Weg 5, CH-8093 Zurich, Switzerland

Multiple glacier readvances, associated with the Egesen Stadial in the Alps, occurred during the YD climate oscillation (Ivy-Ochs et al., 2023 and references therein). As a result, glaciers formed prominent moraine systems and complexes in the valleys and cirques (Ivy-Ochs et al., 2006; 2015; 2023). These moraine systems are crucial geomorphological markers for reconstructing YD glacier fluctuations in the Alps, as glaciers respond sensitively and rapidly to climate changes (Ohmura et al., 1992; Ivy-Ochs et al., 2007; Baroni et al., 2021). Therefore, variations in glacier size reflect changing climate conditions, particularly in temperature and precipitation pattern over time (Kerschner, 2005; Oerlemans, 2005; Schimmelpfennig et al., 2014; Baroni et al., 2021). In addition, the extent of glaciers, glacial landforms, and deposits from different advances allow for the quantitative reconstruction of glaciological and climatological parameters, i.e. equilibrium line altitude (ELA), ELA depression (ΔELA) and temperature decrease (ΔT) compared to the Little Ice Age (LIA) ELA, the paleotemperature of July (T_{jul}) and paleoprecipitation (Ohmura et al., 1992; Kerschner et al., 2000; Kerschner, 2005; Ohmura and Boettcher, 2018; Baroni et al., 2021).

Numerous studies on Egesen moraines across the Alps have been conducted over the past decades (Ivy-Ochs et al., 1996; Kelly et al., 2004; Schindelwig et al., 2012; Schimmelpfennig et al., 2014; Protin et al., 2019; Baroni et al., 2021; Ivy-Ochs et al., 2023 and references therein). Although the extent of the Alpine glaciers during the Egesen stadial is well established in the larger and more prominent glacier systems, the fluctuations and re-advances in smaller tributary valleys still need to be investigated. In particular, understanding the YD remains crucial for exploring the still poorly understood re-advances of glaciers and for interpreting post-LGM glacier dynamics and regional paleoclimate variability in the Alps (Ivy-Ochs et al., 2023). Despite substantial progress, key questions remain about the precise timing and extent of YD glacier fluctuations, particularly in less studied tributary valleys. Additionally, several studies have revealed the importance of local factors, such as valley orientation, hypsometry and catchment area, in modulating glacier responses in addition to overall regional factors (e.g., Schindelwig et al., 2012 and references therein).

With this study, we aim to enhance the understanding of glacier fluctuations in the Alps during the Lateglacial and Early Holocene by focusing on the northern Valaisian Alps. Specifically, we analyze the moraine systems in two tributary valleys west of the Great Aletsch Glacier, namely the Belalp and Luesgenalp valleys (Fig. 1). This setting offers a unique opportunity to test and compare the response of glaciers of different sizes to Younger Dryas climate fluctuations, from the small tributary glaciers to the Great Aletsch Glacier, the largest glacier in the Alps today. Our goal is to determine when they readvanced, how long they stayed in the expanded position, and which climatic deteriorations caused their advances. To achieve this, we conducted detailed surficial geological and geomorphological mapping, established the chronology of glacier fluctuations using surface exposure dating with cosmogenic ^{10}Be, and performed a geomorphology-based reconstruction of the paleoglaciers to determine ELA and ELA depression. These reconstructions allowed us to infer paleotemperature and paleoprecipitation conditions. Finally, we assessed the regional paleoclimatic evolution of the northern Valaisian Alps by comparing our results with existing climate proxies from the broader Alpine region.

Our results provide new detailed insights into the YD advances in these tributary valleys, filling a critical gap in the Alpine paleoclimate record. Furthermore, these geomorphologically based reconstructions offer robust constraints for refining the existing numerical glacier models for the Alps (Seguinot et al., 2018; Jouvet et al., 2017; 2023) and improving simulations of ice field evolution in the region (cf. Leger et al., 2025). By combining high-resolution field mapping with surface exposure dating, this study advances the understanding of how local topography influences glacier sensitivity during abrupt climate shifts and sets a foundation for enhancing model predictions of glacier behavior under climate change scenarios.

2 Study area

The study area is located in the southeastern part of the Bernese Alps in the canton of Valais, Switzerland, covering an area of approximately 9 km^2 (Fig. 1). It includes the south-southeast facing Belalp and Luesgenalp tributary valleys, situated north of Blatten bei Naters and west of the Great Aletsch Glacier. Belalp is a U-shaped valley that extends 5 km in length and up to 2.3 km in width (Fig. 2). It is confined to the north by the Unnerbaech cirque, surrounded by the Grisighorn (3177 m above sea level; asl), Unnerbaechhorn (3554 m asl), and Hostock (3225 m asl) summits (Figs. 1 and 2). This valley hosts the Unnerbaech glacier, which covered an area of 0.3 km^2 in (Christl, et al., 2017) (Linsbauer et al., 2021) (Fig. 2). In contrast, Luesgenalp valley is formed by the Hostock cirque, measuring 3.3 km in length and up to 1.4 km in width. It is enclosed to the west, north and east by the Hostock (3225 m asl), Hülsenhorn (3165 m asl) and Sparrhoru (3020 m asl) peaks (Figs. 1 and 2). The Hostock glacier, which had been present since the Little Ice Age, remained until at least 1973 (Müller et al., 1976). However, according to the Swiss Glacier Inventory of 2016 (Linsbauer et al., 2021), it had completely melted by 2016 (Fig. 2). Additionally,

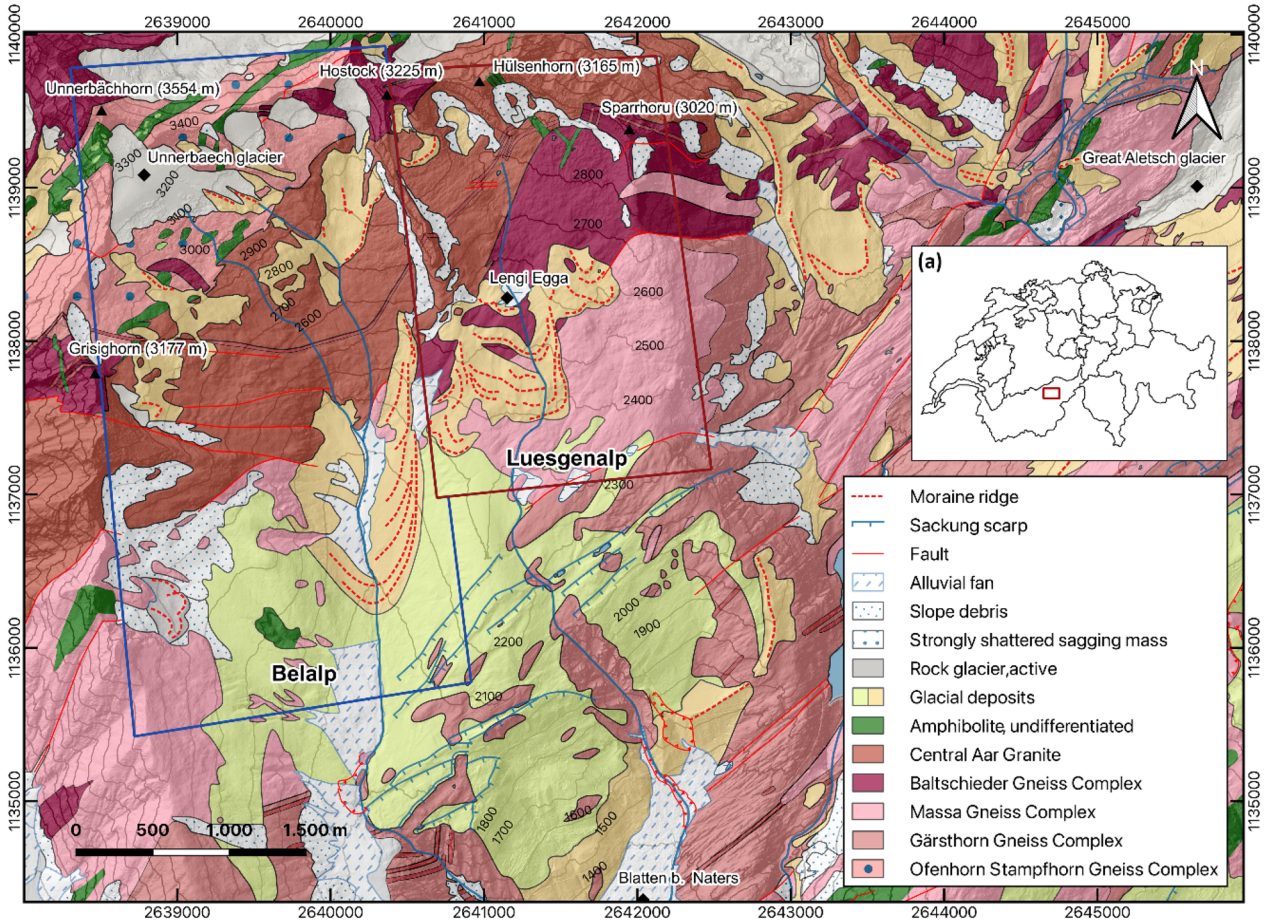

Fig. 1 Geological overview map of the study region (adapted after GA25 geological map sheet 1269 Aletschgletscher (Steck, 2011). Blue and red rectangles show the study sites of the Belalp and Luesgenalp valleys. Inset (a) illustrates the position of the study area in Switzerland (red rectangle). The green-colored glacial deposits are attributed to the LGM, while the light ochre-colored glacial deposits represent Lateglacial to LIA advances

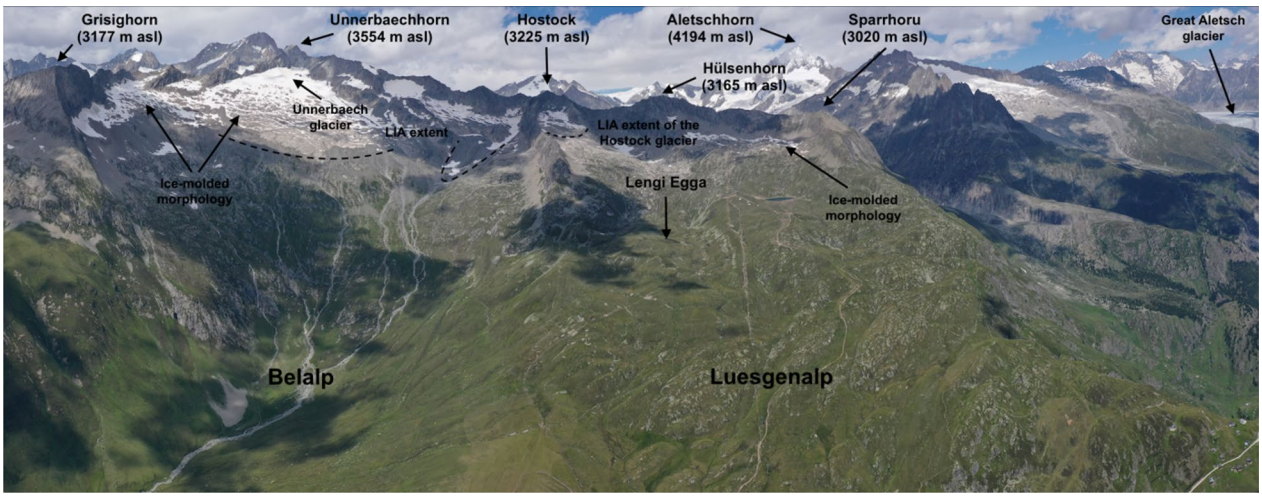

Fig. 2 Unmanned air vehicle picture of the study area. Left, the U-shaped Belalp valley and right the Luesgenalp valley. Dashed lines show the LIA extent of the Unnerbaech and Hostock glaciers for the cirques in the Belalp and Luesgenalp valleys, respectively. View towards the north

a second small cirque, Lengi Egga, is located in the central eastern part of Luesgenalp (Schindelwig et al., 2012) (Figs. 1 and 2).

The crystalline bedrock in the Belalp and Luesgenalp valleys belong to the Aar Massif, part of the Helvetic tectonic unit (Meyer, 2017) and is one of the External Crystalline Massifs of the Alps (e.g. von Raumer et al., 1993). Five major geological units are found at the study sites: the Gärsthorn Gneiss Complex, the Massa Gneiss Complex, the Ofenhorn-Stampfhorn Gneiss Complex, the Baltschieder Granodiorite, and the Central Aar Granite (Fig. 1). The oldest three complexes are classified as pre-Variscan polycyclic metamorphic rocks (Schneeberger et al., 2019). The Gärsthorn Gneiss Complex consists mainly of augen gneiss and coarse-grained two-feldspar gneiss. In contrast, migmatites and migmatitic gneiss form the Massa Gneiss Complex (Berger et al., 2017). At the study area, the Ofenhorn-Stampfhorn Gneiss Complex, comprises of biotite-plagioclase gneiss with magmatitic amphibolite bodies (e.g. Steck, 2011; Berger et al., 2017 and references therein). The younger two units are lower Variscan and upper to post-Variscan intrusive plutonic rocks that were subjected to greenschist-facies metamorphism during Alpine deformation (Steck, 2011; Meyer, 2017; Schneeberger et al., 2019). Quaternary sediments in the central and southern part of the investigation area are of glacial and glaciofluvial origin (Steck, 2011). At Belalp, a moraine complex with multiple ridges is present on the left part of the valley between 2100 and 2550 m asl (Schindelwig et al., 2012), whereas the moraine complex at Luesgenalp is located in the central part between 2300 and 2660 m asl (Fig. 1).

3 Methodology

3.1 Photogrammetry

To reconstruct the glacier fluctuations and to determine the paleoclimate of our study area, we generated a high-resolution digital elevation model (DEM) and orthophotograph with a resolution of 5 cm/pixel for both Belalp and Luesgenalp. Aerial photographs were taken using a DJI Mavic Pro 2 unmanned aerial vehicle (UAV) over the course of 10 flights. The flight missions were planned using Litchi® in Mission Hub (https://flylitchi.com/hub). Each flight was conducted at a height of 200 m above ground and at a speed of 45 km/h. The overlap between photographs within the same flight line was 80%, capturing a photograph every 34 m or approximately every 2.7 s. The distance between two flight lines was 100 m, achieving a lateral overlap of 60%. The collected images were processed at the Institute of Geology in Bern using Agisoft Metashape® photogrammetry software (Agisoft, 2014, 2017).

3.2 Detailed mapping

The surficial geology of the study area was mapped by combining field and remote mapping techniques. Field mapping was conducted during the summers of 2022 and 2023, systematically crossing the study area multiple times following the approach proposed by Chandler et al. (2018). For the remote mapping, we utilized orthophotographs and DEMs generated through photogrammetry, the GA25 geological map sheet 1269 Aletschgletscher (Steck, 2011), and the GK500-Tekto map (Tektonische Karte der Schweiz, 1:500,000. 2005). Additionally, we created a red relief image map (RRIM) following Daxer (2020). This type of map highlights concavities and convexities on a surface of topographic features (Chiba et al., 2008; Daxer, 2020), which facilitated the identification of linear landforms. Detailed surficial geological and RRIM maps were generated using QGIS®.

3.3 Surface exposure dating

By applying surface exposure dating with cosmogenic nuclides (e.g. ^{10}Be), the glacial deposits and landforms can be dated, determining how long they are exposed on the surface (Ivy-Ochs and Kober, 2008). This method is often used to establish the time of deposition of boulders on moraines or to determine since when a glacially-polished bedrock is no longer covered by ice (Kelly et al., 2004). As moraines mark glacier culminations of the past, dating these landforms allows to reconstruct chronologies of the past glacial environments and link them to past climatic fluctuations (Kerschner and Ivy-Ochs, 2008; Schindelwig et al., 2012). Defining glacial chronologies and comparing them with glaciological and climatological parameters improve our understanding of past climatic changes and can contribute to assessing the impact of the ongoing climate warming (e.g. Rasmussen et al., 2014; Schimmelpfennig et al., 2014).

To determine the timing of glacier fluctuations in our study area, we applied surface exposure dating with the cosmogenic nuclide ^{10}Be. 14 granitic samples were collected from moraine crests at Luesgenalp for cosmogenic ^{10}Be analysis. In addition, we recalculated 21 exposure ages originally published by Schindelwig et al. (2012) for the Belalp valley, based on original raw data. For context and comparison, we also use exposure ages from other Alpine valleys reported by Ivy-Ochs et al. (2023), who recalculated those from earlier primary sources. The samples at Luesgenalp were collected from the top surfaces of boulders using an angle grinder, hammer, and chisel, following the strategies defined in previous studies (e.g. Akçar et al., 2011). For each sample, we recorded geographic information, boulder height, sample thickness, and topographic shielding (Dunai, 2010) (Table 1).

Table 1 Sample information from the Belalp and the Luesgenalp valleys

Sample name	Altitude (m a.s.l.)	Latitude, °N (DD.DD) WGS84	Longitude, °E (DD.DD) WGS84	Boulder height (m)	Sample thickness (cm)	Factor of shielding correction	Surface orietation (azimuth/dip)
LUES-1	2461	46.39006	7.97827	1.4	4.5	0.9890	Flat
LUES-2	2465	46.38978	7.97100	2.0	4.0	0.9898	Flat
LUES-3	2458	46.38940	7.97144	1.0	5.0	0.9898	Flat
LUES-4	2421	46.38824	7.97452	2.2	5.0	0.9951	Flat
LUES-5	2546	46.39398	7.97573	0.8	4.0	0.9803	Flat
LUES-6	2559	46.39363	7.97414	0.8	3.5	0.9886	Flat
LUES-7	2569	46.39400	7.97283	1.4	5.0	0.9812	Flat
LUES-8	2567	46.39426	7.97197	1.2	4.0	0.9812	Flat
LUES-9	2604	46.39432	7.96960	1.0	5.0	0.9720	Flat
LUES-10	2606	46.39454	7.96958	1.0	5.0	0.9720	Flat
LUES-11	2607	46.39462	7.96959	0.5	4.5	0.9720	Flat
LUES-12	2520	46.39135	7.96978	1.6	4.0	0.9896	Flat
LUES-13	2525	46.39245	7.97721	0.5	4.0	0.9845	Flat
LUES-14	2522	46.39233	7.97717	0.7	4.0	0.9845	Flat
*VBA-1	2239	46.38540	7.96544	1.6	5.0	0.9890	Flat
*VBA-2	2238	46.38531	7.96548	1.2	5.0	0.9890	Flat
*VBA-3	2275	46.38613	7.96578	1.6	5.0	0.9680	Flat
*VBA-4	2507	46.39249	7.96541	1.0	5.0	0.9670	Flat
*VBA-5	2460	46.39141	7.96547	0.6	2.0	0.9370	Flat
*VBA-6	2330	46.38804	7.96532	1.0	5.0	0.9840	Flat
*VBA-11	2172	46.38221	7.96417	1.5	2.0	0.9830	Flat
*VBA-12	2205	46.38385	7.96526	1.7	2.0	0.9830	Flat
*VBA-13	2160	46.38159	7.96366	1.8	4.0	0.9750	Flat
*VBA-14	2148	46.38111	7.96294	1.5	3.0	0.9750	Flat
*VBA-15	2143	46.38043	7.96335	1.5	5.0	0.9750	Flat
*VBA-16	2146	46.38054	7.96346	1.0	3.5	0.9750	Flat
*VBA-17	2244	46.38719	7.96320	3.0	1.5	0.9760	Flat
*VBA-18	2378	46.38961	7.96460	1.2	3.0	0.9760	Flat
*VBA-19	2424	46.39070	7.96480	1.8	2.0	0.9830	Flat
*VBA-20	2426	46.39075	7.96480	2.0	2.5	0.9830	Flat
*VBA-22	2122	46.37851	7.96380	1.2	1.5	0.9750	Flat
*VBA-23	2138	46.37917	7.96435	1.0	4.0	0.9720	Flat
*VBA-24	2166	46.38041	7.96530	1.1	4.0	0.9730	Flat
*VBA-25	2158	46.38006	7.96500	2.2	4.0	0.9730	Flat
*VBA-26	2139	46.37922	7.96440	1.5	3.0	0.9720	Flat

* Schindelwig et al., 2012

The height of the sampled boulders ranged from 0.5 to 2.2 m, and sample thickness varied between 3.5 and 5 cm.

The sample preparation was conducted at the Surface Exposure Dating Laboratory of the University of Bern. We crushed and sieved the samples to a grain size of 250–400 µm, then isolated and purified the quartz following the technique described by Akçar et al. (2017), after Kohl and Nishiizumi (1992). ^{10}Be was subsequently extracted from the samples applying the method described in Akçar et al. (2012). The accelerator mass spectrometry (AMS) measurements of ^{10}Be/^{9}Be ratios were performed on the MILEA system (Maxeiner et al., 2019) at the ETH AMS facility in Zurich. A half-life of 1.39 Ma for ^{10}Be (Chmeleff et al., 2010; Korschinek et al., 2010) was used, and the results were normalized to the ETH in-house standards S2007N and S2010N (Christ and Kubik, (Christl, et al., 2013)). The ^{10}Be/^{9}Be ratios were then corrected with the long term-weighted average full process blank ratio of $(3.34 \pm 0.23) \times 10^{-15}$. The ^{10}Be exposure ages were determined using the version 3 of the

online exposure age calculator, formerly known as the CRONUS-Earth online exposure calculator (http://hess.ess.washington.edu/math/v3/v3_age_in.html) written by Balco et al. (2008). We applied altitude/latitude scaling for the production rate according to the time-dependent Lal (1991)/Stone (2000) scheme. Our calculations accounted for sample thickness (applying an exponential attenuation length of 160 g/cm^2), topographic shielding (Dunne et al., 1999), an erosion of 1 mm/ka (André, (Andre, and André, 2002)), and a rock density of 2.65 g/cm^3. Shielding correction factors were calculated after (Tikhomirov et al., 2014). Sample information is detailed in Table 1. No snow cover correction was applied to the exposure ages, we specifically selected large, high-standing boulders situated on moraine crests and elevated above the surrounding topography. These boulders are likely to be windswept and free of persistent snow cover (Gosse and Phillips, 2001; Ye et al., 2023). The same settings were used for recalculating the data of Belalp valley published in Schindelwig et al. (2012). In addition, we analyzed the data using the probabilistic cosmogenic age analysis tool (P-CAAT) (Dortch et al., 2022), which runs in a MATLAB environment, to identify potential outliers and obtain probability density function plots of the ^{10}Be exposure ages.

3.4 Glacier reconstruction

In this study, we applied geomorphology-based glacier reconstruction (cf. James et al., 2019). The reconstruction of the Unnerbaech paleoglacier at Belalp valley and the Hostock paleoglacier at Luesgenalp valley was conducted using the toolbox GlaRe® (Pellitero et al., 2016) in ArcGIS®. The SwissALTI3D® relief map, with a resolution of 0.5 m per pixel, served as the base map for glacier reconstruction. Where present, moraines were used to confine the glacier margin. We reconstructed these paleoglaciers at their maximum extent and the Little Ice Age (LIA). Subsequently, ELA was calculated using the ELA® toolbox (Pellitero et al., 2015) with the accumulation area ratio (AAR) technique (Porter 1975). We determined the ELAs using AAR ratios between 0.5 and 0.8. In this study, we used the ELAs obtained with an AAR ratio of 0.67, as it is the best-fitting value for valley and cirque glaciers in the Alps according to Gross et al. (1978). We then calculated the ELA depressions. Using these depressions, the temperature decreases compared to the LIA were estimated by applying a temperature gradient of 0.65 °C/100 m.

To reconstruct the paleotemperature for the hottest month, July (T_{jul}), we used chironomid assemblages at Lago Piccolo di Avigliana in Italy (365 m asl; 45° 30 N 45°03′ N 7°23′ E), located 150 km southeast of Belalp and Luesgenalp. Larocque and Finsinger, (2008) determined a T_{jul} of about 16.0 °C at this location. This temperature was adjusted to the ELA of the maximal paleoglacier extent at our study area. The annual paleo-precipitation (P_{ann}) at the ELA was defined using the temperature/precipitation equations described in Ohmura and Boettcher (2018). We calculated the precipitation with both the linear approximation ($P_{ann} = 264.1\ T + 957$) and the quadratic approximation ($P_{ann} = 5.82\ T^2 + 230\ T + 966$), where T corresponds to T_{jul}.

4 Results

4.1 Surficial geology

The Belalp and Luesgenalp valleys show a glacially overprinted landscape, and glacial deposits and landforms dominate the area (Fig. 3). Both valleys have undergone human impact during the last century (Figs. 3 and 4). For example, several erratic boulders in the Belalp valley were destroyed or moved during the construction of the ski resort during the 2000's (Fig. 4a). In the Luesgenalp valley, moraines were partially destroyed to build ski tracks and cable car (Fig. 4b and c). In addition, a 20,000 m^2 large artificial lake was built between 2008 and 2011 during which moraines in the eastern part of Luesgenalp were destroyed (Fig. 4b and c).

In the northern halves of the two valleys, the bedrock either outcrops with an ice-molded morphology or is overlain by a thin veneer of till (Figs. 2 and 3). In the northern half of the Belalp valley, the bedrock consists of the Ofenhorn-Stampfhorn Gneiss Complex and Central Aar Granite. In the southern half, bedrock outcrops are sporadic and comprise the Massa Gneiss Complex in the central part, Baltschieder Granodiorite in the east, Gärsthorn Gneiss Complex in the southeast. In the Luesgenalp valley, the bedrock is made of Central Aar Granite in the north, Baltschieder Granodiorite in the central part, and Massa Gneiss Complex in the south (Figs. 1 and 3).

The Quaternary deposits and landforms are largely present at the study area and are covered by vegetation, which consists of grass and sporadic small shrubs. Along the flanks and in the southern parts of Belalp and Luesgenalp valleys, lateral and terminal moraines dominate the landscape (Figs. 3, 5, 6 and 7). A total of 33 moraines were mapped across the study area, consisting of 23 terminal moraines and 10 lateral moraines. The length of the terminal moraines varies between 50 and 1250 m, the width between 10 and 40 m and the height is 0.5 m to 6 m. The lateral moraines, on the other hand, have length of 60 m to 2 km, widths of 30 m to 100 m and heights of 3 m to 15 m. Lateral moraines thus tend to be wider and higher than the terminal moraines.

In this study, the relative chronology of the moraines was used to differentiate glacial deposits into "older"

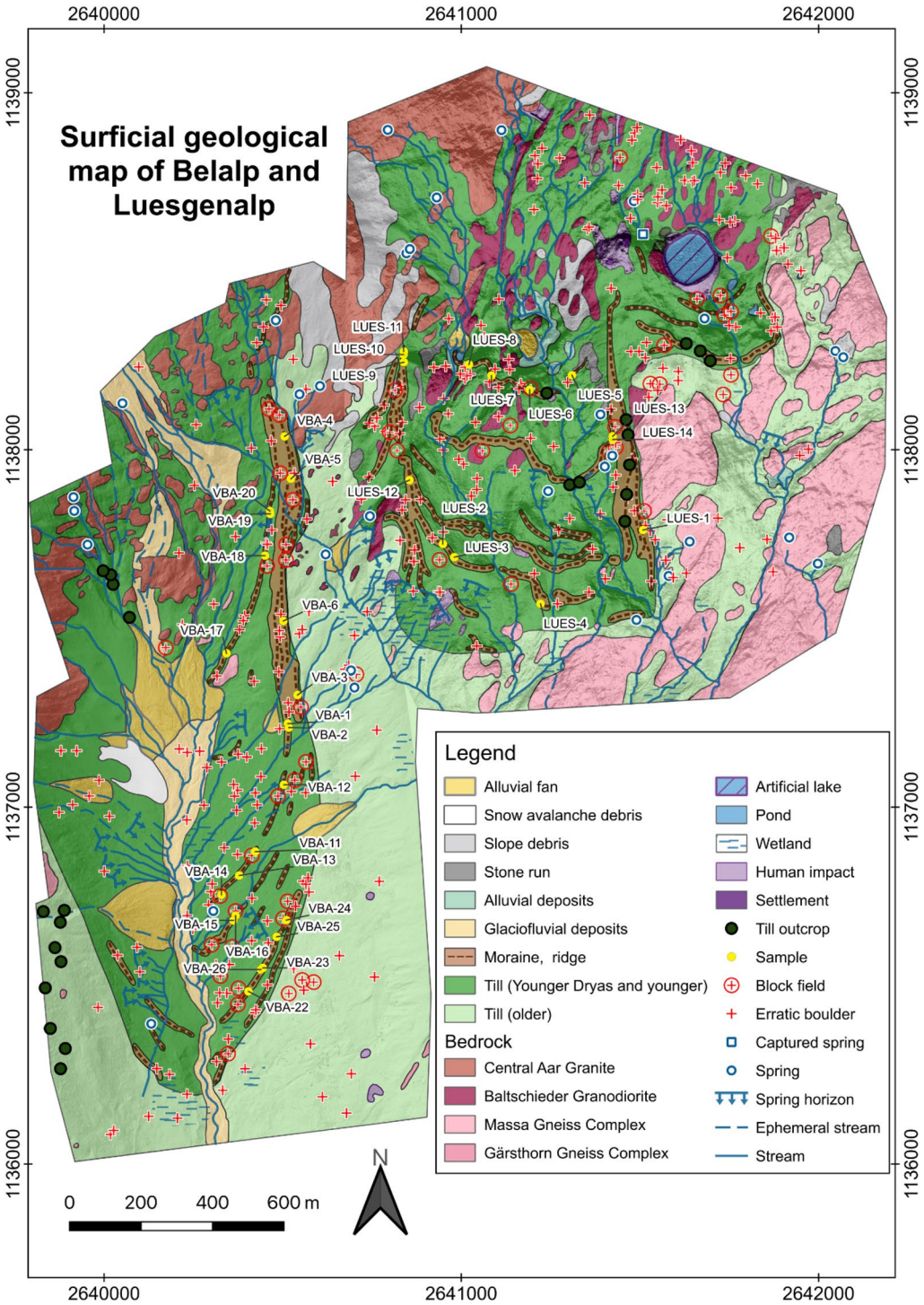

Fig. 3 Surficial geological map of the Belalp and Luesgenalp valleys

and "Younger Dryas and younger" till by using the cosmogenic ^{10}Be chronology after Schindelwig et al. (2012) (Fig. 3). Till outcrops are generally small, less than around 100 m^2, except for two man-made outcrops, each approximately 1000 m^2, located near the artificial lake in the Luesgenalp valley. They are mainly confined along the stream and on the right flank at the Belalp valley, and around the left lateral moraine at the Luesgenalp valley

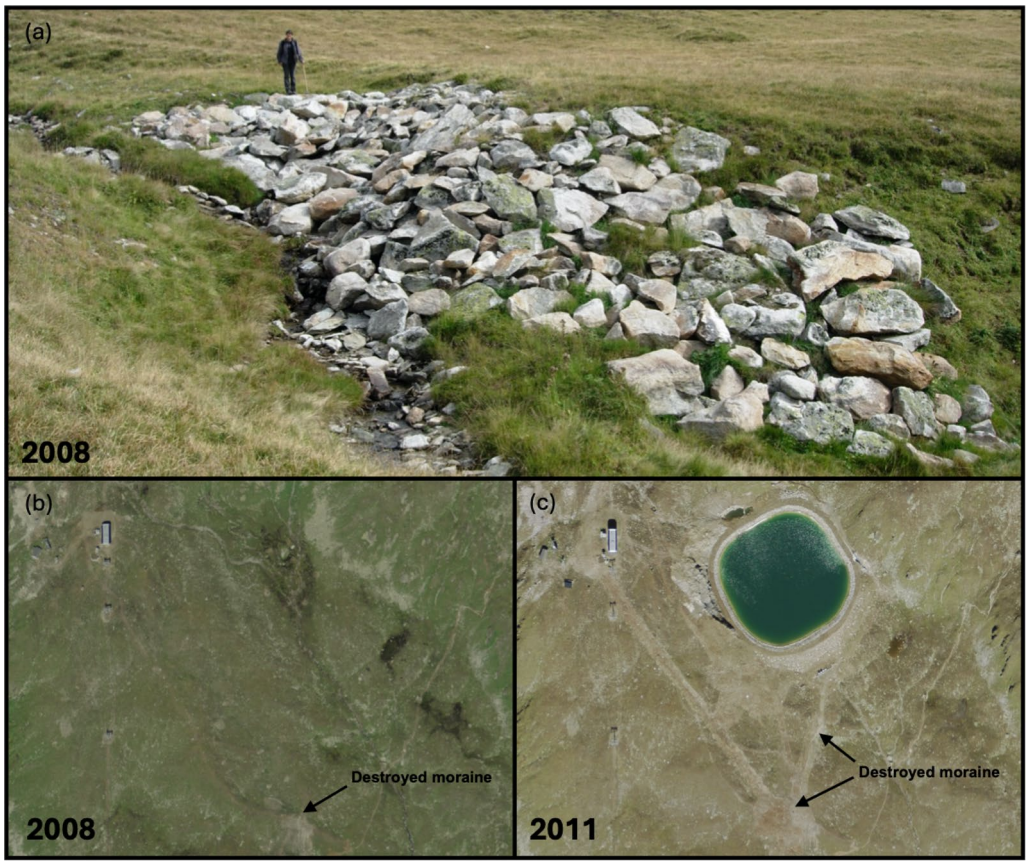

Fig. 4 Human impact at the study area. **a** Example of destroyed and moved erratic boulders in the Belalp valley mapped as human impact in Fig. 3 (picture modified after Schindelwig et al. (2012). View towards the east. **b** Situation in the eastern part of the Luesgenalp valley in 2008. **c** Situation in the eastern part of the Luesgenalp valley after the completion of the artificial lake in 2011

(Fig. 3). The till is composed of poorly sorted crystalline clasts in a silty to sandy matrix. Across the study area, crystalline erratic boulders ($\geq 1 m^3$) and block fields are disseminated and lie predominantly on the till (Fig. 3). At the Luesgenalp valley, we mapped 14 flutes oriented nearly north–south, reflecting the ice flow direction of the paleoglacier, as they are always aligned parallel to the glacier (Chandler et al., 2018 and references therein). They range from 40 to 200 m length and up to 5 m in width (Fig. 7). At the Belalp valley, clast-supported glaciofluvial deposits are present along the current bed of the mainstream (Fig. 3).

Along the flanks of the Unnerbächhorn (Belalp) and Hostock cirques (Luesgenalp), and to the north of Lengi Egga in the Luesgenalp, slope debris covers the till and bedrock (Figs. 1, 2 and 3). In the central of the Luesgenalp valley, we mapped narrow, elongated stone runs composed of cobbles and boulders up to 1 m^3 in size (Fig. 3). Based on their morphology and alignment, we interpret them as relict periglacial deposits, rather rockfall deposits resulting from adjacent cliffs (cf. Kim and Ma, 2023). A snow avalanche debris deposit, approximately 250 m long, 100 m wide, and a few meters high, is located on the east side of the Belalp valley (Fig. 3). The accumulation of debris from repeated snow avalanches over time can result in the formation of snow avalanche ridges (Akçar et al., 2007). However, the absence of ridge morphology in this debris suggests that snow avalanche activity in this area is either sporadic or has only recently begun. Furthermore, the lack of vegetation on the surface of the debris indicates that the process is still active (Fig. 2).

In the study area, streams and ephemeral streams are distributed over the entire area and springs and spring horizons are frequent (Fig. 3). Smaller streams dry up during summer. Alluvial fans are up to 400 m in length and 200 m in width but are more and larger in size at Belalp (Fig. 3). The alluvial fans at the Luesgenalp valley are situated at the small cirque of Lengi Egga and have a length of about 100 m and a width of about 80 m. The overdeepened part of the cirque is filled by alluvial deposits (Fig. 3). Ephemeral wetlands are present at the floor of the Belalp valley and in the southern part of the

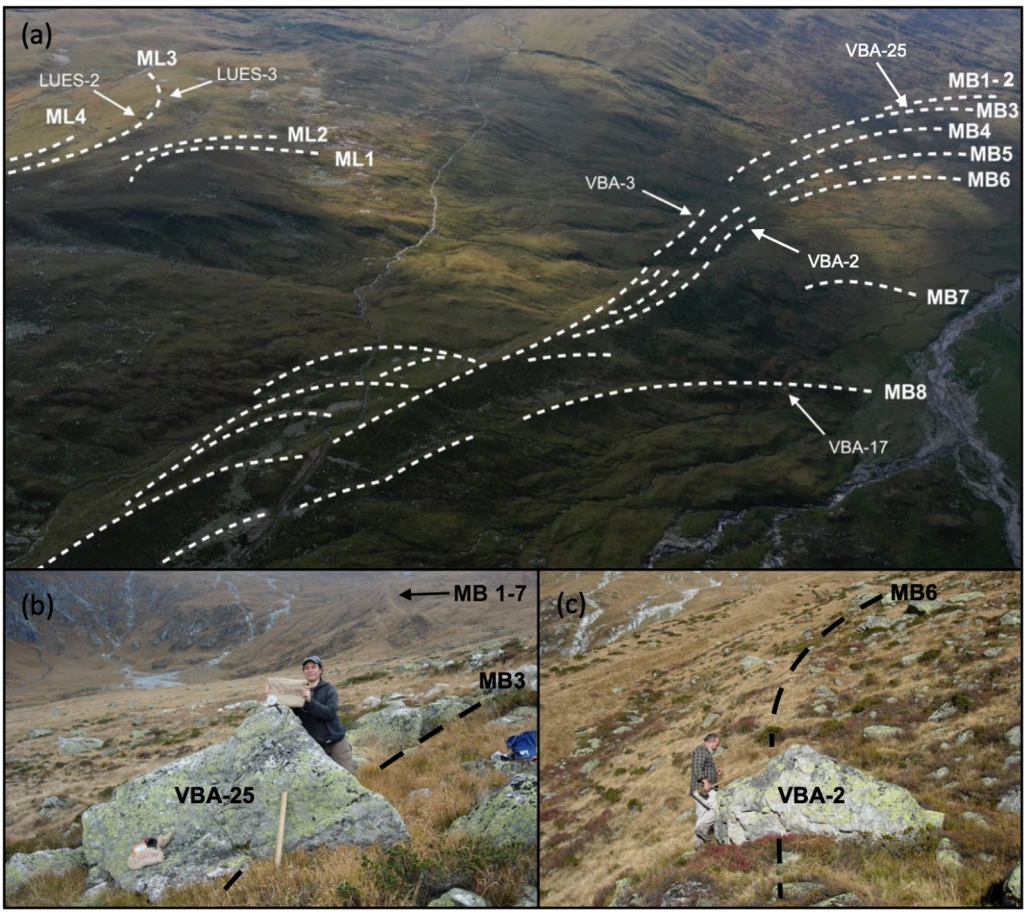

Fig. 5 Field photographs of the Belalp valley. **a** View on the left lateral moraine complex and the latero-terminal moraines MB1 to MB8 in the Belalp valley. In the upper left of the picture the lower western part of the moraines ML1 to ML4 in the Luesgenalp valley are visible. View toward southeast. **b** Boulder VBA-25 on moraine MB3 sampled by Schindelwig et al. (2012) (View towards the north). **c** Boulder VBA-2 on moraine MB6 sampled by Schindelwig et al. (2012) (view towards the north)

Luesgenalp valley (Fig. 3). They are formed when the uppermost part (< 20 cm) of the till veneer is saturated due to snow melt in spring and early summer. The six ponds were identified at the Luesgenalp valley: three at Lengi Egga and three near the artificial lake. They are less than 1.5 m deep and cover a maximal area of 400 m^2 (Fig. 3).

4.2 Surface exposure dating

The amount of dissolved quartz, ^{9}Be spike, AMS ratio, error in AMS ratio, ^{10}Be concentration and exposure ages within 1σ uncertainties are listed in Table 2. At the Belalp valley, the recalculated ^{10}Be exposure ages range from 9.7 ± 1.0 ka to 14.8 ± 0.6 ka (after Schindelwig et al., 2012). At the Luesgenalp valley, ^{10}Be concentrations vary between (29.74 ± 0.82) × 10^4 at/g and (36.46 ± 0.55) × 10^4 at/g, and the exposure ages between 10.6 ± 0.4 ka and 12.9 ± 0.4 ka. The exposure ages include the corrections for sample thickness, dip of rock surface, topographic shielding and erosion. No correction for snow cover was applied. The reported uncertainties are internal (cf. Balco et al., 2008), i.e. do not include the production rate errors. Whereas the uncertainties given in parenthesis include the production rate errors (external sensu Balco et al., 2008) (Table 2). In the discussion section, we use the exposure ages with external uncertainties when we compare our dataset with other climate proxies.

4.3 Glacial history

4.3.1 Belalp valley

In the Belalp valley, we identified at least eight glacier advances based on geomorphological evidence (Fig. 3 and 7). These moraines are numbered in chronological order, from the outermost (MB1) to the innermost (MB8), thus from the morphostratigraphically oldest to youngest. Moraines MB1 to MB8 are preserved on the left lateral valley side, whereas only moraines MB1, MB2, and MB3 were found on the right lateral side (Fig. 7). Moraines

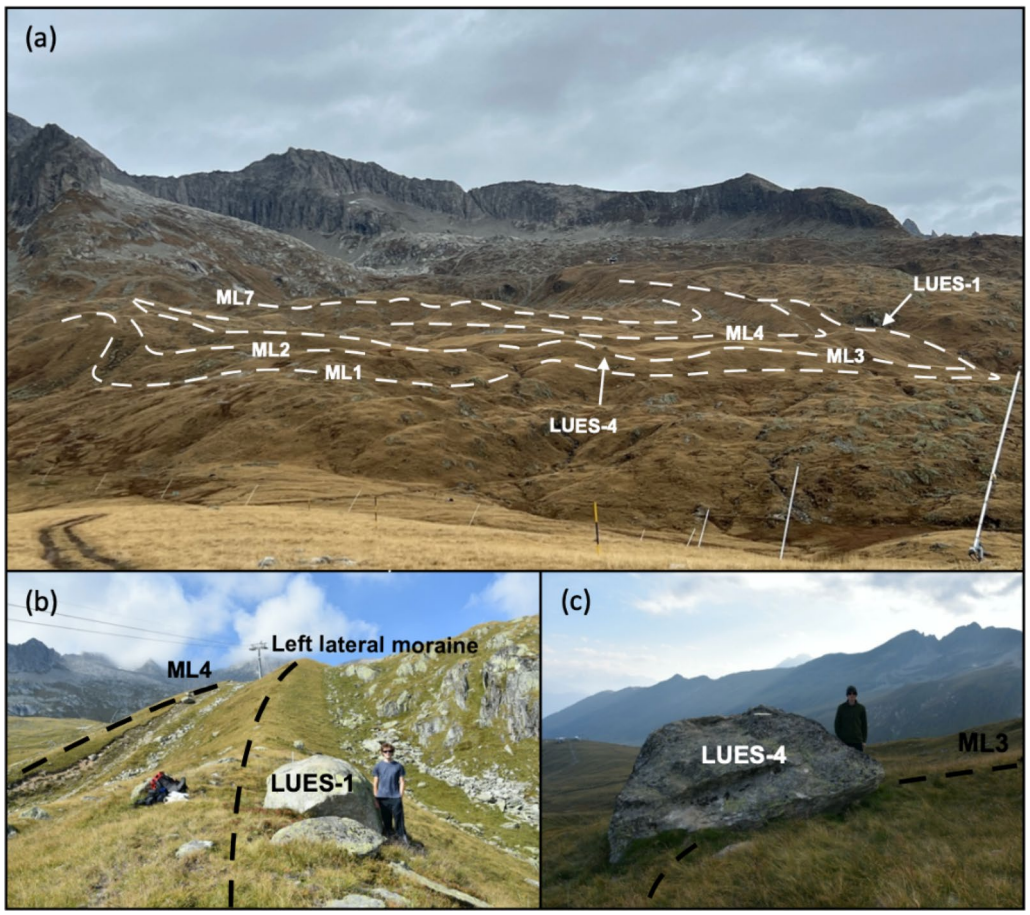

Fig. 6 Field photographs of the Luesgenalp valley. **a** View on the terminal moraines ML1, ML2, ML3, ML4 and ML7 south of Lengi Egga (Fig. 2 for reference). View towards the north-northeast. **b** Boulder LUES-1 on the left lateral moraine east of Lengi Egga (view towards the north). **c** Boulder LUES-4 on moraine ML3 (view towards the west)

MB1 to MB7 form a lateral moraine complex on the left lateral side, extending for 2 km from 2100 m asl and 2550 m asl. In the upper part of the moraine complex, between 2550 m asl and ca. 2400 m asl, the moraines intertwine and bifurcate (Fig. 7A). Making them difficult to distinguish. They reach a maximal height of ca. 15 m and width of ca. 100 m. In the central and lower part of the complex, between ca. 2390 m asl and 2100 m asl, moraines MB1-7 gradually intermingle from each other, forming individual terminal ridges (Fig. 7 and B).

The observed superposition of the moraine complex are characteristic of composite lateral moraines, which are commonly found in the Valaisian Alps (cf. Schneebeli, 1976; Le Roy et al., 2024). Such moraine structures are formed through successive glacier fluctuations at the lateral margin, where advancing ice deposits sediment on top of pre-existing moraines. If the advance is less extensive than the previous one, or if the ice flow is redirected laterally due to changes in bed morphology or constrained valley walls, the glacier overtops the older moraine ridge, adding new sediment layers (Schneebeli, 1976; Winkler, 2009; Lukas et al., 2012; Le Roy et al., 2024). Over time, this repeated "overtopping" behavior archives multiple glacier advances within the same lateral moraine, resulting in complex, fragmented structures. This process has been well-documented in the Alps, such as the Holocene (sensu lato) lateral moraines of the Findelen Glacier, where advances during the Little Ice Age reworked older moraine deposits (Röthlisberger, 1976; Lukas et al., 2012; Le Roy et al., 2024). The composite structure observed in the Belalp valley is thus interpreted as evidence of multiple glacier fluctuations, resulting in the fragmented and overlapping moraine ridges. Schindelwig et al. (2012) dated four boulders on this left lateral moraine complex (recalculated exposure ages); VBA-3 (14.8 ± 0.6 ka), VBA-4 (10.2 ± 0.7 ka), VBA-5 (11.7 ± 0.6 ka) and VBA-6 (12.1 ± 0.6 ka) (Fig. 5 and 7; Table 2). However, based on their position, it is not possible to associate them with any specific terminal moraine MB1 to MB7 (Figs. 7A and B). Schindelwig et al. (2012) suggest

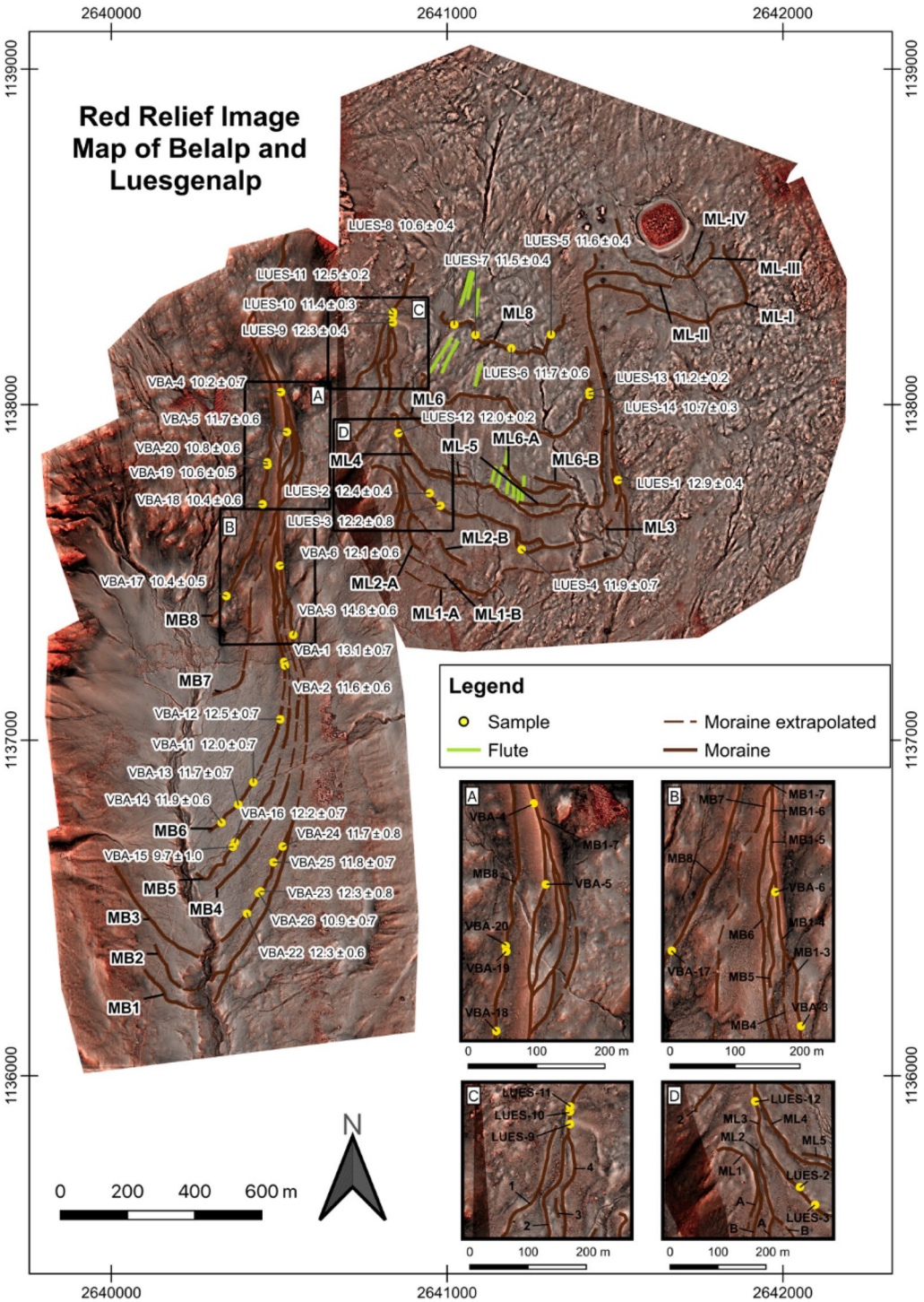

Fig. 7 Red Relief Image Map of the Belalp and Luesgenalp valleys, with sample ages and moraine names indicated. Black rectangles on the map highlight the zoomed-in areas shown in pictures A-D

that VBA-4 was likely affected by post-depositional processes such as displacement or exhumation, as it yielded a significantly younger exposure age compared to other boulders on the same moraine (cf. Akçar et al., 2011); therefore, we excluded this boulder from further discussion. Moraine MB1 is the outermost terminal moraine in

Table 2 *Cosmogenic ^{10}Be data of the samples from Belalp and Luesgenalp valleys*

Sample name	Quartz dissolved (g)	^{9}Be spike (mg)	AMS ratio ($\times 10^{-13}$)	Error in AMS ratio (%)	^{10}Be (10^4 at/g)	Erosion corrected ($\varepsilon = 1.0$ mm ka^{-1}) exposure age (ka)	
LUES-1	50.1638	0.1985	13.29	3.15	35.05 ± 1.11	12.9 ± 0.4	(1.1)
LUES-2	50.0562	0.1993	12.68	3.34	33.64 ± 1.13	12.4 ± 0.4	(1.0)
LUES-3	49.6972	0.1985	12.32	6.41	32.80 ± 2.11	12.2 ± 0.8	(1.2)
LUES-4	51.0760	0.1932	12.39	5.68	31.24 ± 1.78	11.9 ± 0.7	(1.1)
LUES-5	49.9168	0.1898	12.90	3.71	32.69 ± 1.22	11.6 ± 0.4	(1.0)
LUES-6	50.9248	0.1968	13.08	5.15	33.68 ± 1.74	11.7 ± 0.6	(1.1)
LUES-7	50.0028	0.1996	12.36	3.33	32.87 ± 1.10	11.5 ± 0.4	(1.0)
LUES-8	50.0079	0.1986	11.41	3.76	30.19 ± 1.14	10.6 ± 0.4	(0.9)
LUES-9	49.9755	0.1983	13.46	3.33	35.60 ± 1.19	12.3 ± 0.4	(1.0)
LUES-10	49.9629	0.1986	12.39	2.19	32.82 ± 0.72	11.4 ± 0.3	(0.9)
LUES-11	50.1047	0.2001	13.69	1.50	36.46 ± 0.55	12.5 ± 0.2	(1.0)
LUES-12	50.0500	0.1896	13.42	1.50	33.88 ± 0.51	12.0 ± 0.2	(0.9)
LUES-13	49.9895	0.1994	11.75	1.96	31.24 ± 0.61	11.2 ± 0.2	(0.9)
LUES-14	49.9710	0.1989	11.21	2.76	29.74 ± 0.82	10.7 ± 0.3	(0.9)
*VBA-1	51.3337	0.3044	8,63	5.1	30.47 ± 1.59	13.1 ± 0.7	(1.2)
*VBA-2	50.6890	0.3032	7,55	4.9	26.81 ± 1.35	11.6 ± 0.6	(1.1)
*VBA-3	50.1619	0.3101	9,40	3.9	34.67 ± 1.38	14.8 ± 0.6	(1.3)
*VBA-4	50.3689	0.3024	7,66	6.4	27.28 ± 1.79	10.2 ± 0.7	(1.0)
*VBA-5	49.9685	0.3042	8,43	4.6	30.53 ± 1.44	11.7 ± 0.6	(1.1)
*VBA-6	50.0468	0.3032	8,22	5.0	29.60 ± 1.52	12.1 ± 0.6	(1.1)
*VBA-11	57.3627	0.2808	9,21	5.5	26.88 ± 1.51	12.0 ± 0.7	(1.1)
*VBA-12	46.3229	0.3051	7,41	5.5	28.95 ± 1.64	12.5 ± 0.7	(1.2)
*VBA-13	57.4723	0.2871	8,54	5.5	25.38 ± 1.43	11.7 ± 0.7	(1.1)
*VBA-14	53.6796	0.3046	7,65	5.1	25.77 ± 1.35	11.9 ± 0.6	(1.1)
*VBA-15	51.5483	0.3044	5,84	9.7	20.30 ± 2.04	9.7 ± 1.0	(1.2)
*VBA-16	50.0859	0.3041	7,31	5.2	26.32 ± 1.41	12.2 ± 0.7	(1.1)
*VBA-17	51.2960	0.3035	6,89	4.6	24.14 ± 1.15	10.4 ± 0.5	(0.9)
*VBA-18	43.0575	0.3029	6,31	5.4	26.20 ± 1.46	10.4 ± 0.6	(1.0)
*VBA-19	39.7133	0.3045	6,18	4.9	27.96 ± 1.42	10.6 ± 0.5	(1.0)
*VBA-20	48.2637	0.2943	7,85	5.8	28.44 ± 1.69	10.8 ± 0.6	(1.0)
*VBA-22	50.0867	0.3031	7,40	4.5	26.56 ± 1.23	12.3 ± 0.6	(1.1)
*VBA-23	50.6423	0.2999	7,50	6.5	26.35 ± 1.76	12.3 ± 0.8	(1.3)
*VBA-24	50.0641	0.4943	4,44	6.8	25.52 ± 1.82	11.7 ± 0.8	(1.2)
*VBA-25	50.6108	0.2989	7,29	5.5	25.52 ± 1.45	11.8 ± 0.7	(1.1)
*VBA-26	50.1216	0.3049	6,49	6.5	23.32 ± 1.57	10.9 ± 0.7	(1.1)

* Schindelwig et al., 2012

this valley (Fig. 7). The ridge is broad-crested and reaches a height of 1 m on the western side. MB1 marks the maximum extent and the lowest position (2080 m asl) of the Unnerbaech paleoglacier (cf. Fig. 2). The moraine can be traced for ca. 400 m from the west to the east side of the valley. Moraine MB2 is a terminal moraine 50 m north of MB1, ca. 1 m high and 300 m long. MB1 and MB2 merge into a single moraine ridge on the left-hand side of the valley at 2100 m asl, forming the lowermost part of the moraine complex. The combined moraine MB1-2 extends for ca. 450 m towards the northeast. The moraine ridge consists of a clast-supported openwork deposit, forming a small hummock approximately 0.3 m in height. Embedded within the moraine are aligned crystalline boulders, some up to 2 m long and 1 m high.

Approximately 100 m north of MB2, MB3 is a well-preserved terminal moraine, which extends down to ca. 2100 m asl (Fig. 7). This moraine is ca. 900 m long, ca. 1 m

high, up to 10 m wide and broad-crested. MB3 intercepts moraine MB1-2 at a low angle at ca. 2175 m asl and continues as MB1-3 for ca. 700 m as a fragmented moraine towards the northeast. Schindelwig et al. (2012) sampled five boulders on the moraine MB3 (recalculated exposure ages): VBA-22 (12.3 ± 0.6 ka), VBA-23 (12.3 ± 0.8 ka), VBA-24 (11.7 ± 0.8 ka), VBA-25 (11.8 ± 0.7 ka), VBA-26 (10.9 ± 0.7 ka) (Figs. 3, 5b and 7; Table 2). The probability density function plot shows a unimodal distribution with a tight peak, giving a weighted mean age of 11.8 ± 0.3 (± 1.0) ka.

MB4 is a left latero-terminal moraine that separates from MB1-4 complex at ca. 2330 m asl and disappears at 2120 m asl (Figs. 5a and 7B). The ridge is ca. 900 m long but is highly disintegrated and only partially preserved. It is marked by an array of boulders ranging from 0.5 to 1 m in height.

Ridge MB5 is a 1 km long left latero-terminal moraine 60 m north of MB4 (Fig. 7), with its terminal part extending down to 2120 m asl, where it is cut by glaciofluvial deposits from the stream (Fig. 3). The terminal and upper parts of the ridge are well preserved. They are ca.1.5 m high, up to 15 m wide and narrow-crested. In contrast, the central section is almost completely eroded. This moraine is composed of a clast rich sandy till and contains crystalline boulders up to 1 m long and 0.5 m high. Ridge MB5 joins the moraine complex MB1-4 at a low angle at ca. 2335 m asl and continues northward as MB1-5 (Figs. 5a and 7B). Schindelwig et al. (2012) dated two boulders on moraine MB5 (recalculated exposure ages): VBA-15 and VBA-16 with exposure ages of 9.7 ± 1.0 ka and 12.2 ± 0.7 ka, respectively (Table 2). We excluded VBA-15 from further discussion, as this pyramid-shaped boulder may have experienced toppling, according to Schindelwig et al. (2012). The age of MB5 is 12.2 ± 0.7 (1.1) ka.

Moraine MB6 is a 950 m long, well-defined latero-terminal moraine (Figs. 5a and 7). It branches off from the moraine complex MB1-6 at an altitude of ca.2370 m asl and descends to 2140 m asl (Fig. 7B). Ridge MB6 is narrow-crested, up to 1 m high and 10 m wide. A total of six samples were collected on moraine MB6, yielding exposure ages of 13.1 ± 0.7 ka (VBA-1), 11.6 ± 0.6 ka (VBA-2), 12.0 ± 0.7 ka (VBA-11), 12.5 ± 0.7 ka (VBA-12), 11.7 ± 0.7 ka (VBA-13), and 11.9 ± 0.6 ka (VBA-14) (recalculated ages from Schindelwig et al., 2012) (Figs. 5c and 7; Table 2). The weighted mean age of MB6 is 12.1 ± 0.3 (1.0) ka.

Ridge MB7 is a highly disintegrated and partially preserved latero-terminal moraine. MB7 is ca. 600 m long, ca. 0.5 m high, and extends from ca. 2190 m asl to ca. 2390 m asl, where it intersects the moraine complex MB1-6 (Fig. 7). The moraine continues northward as MB1-7 (Fig. 7B). This ridge is approximately 400 m upstream from MB6 and is the last moraine to have reached the valley floor (Figs. 3, 5a and 7).

MB8 is the innermost ridge in the Belalp valley and is a well-defined and preserved left latero-terminal moraine (Fig. 7). The ridge runs continuously from ca. 2220 m asl to ca. 2700 m asl near the eastern end of the Unnerbaech cirque. MB8 is cut at ca. 2220 m asl by the alluvial fans present at the beginning of the valley floor (Fig. 3). The moraine is 1250 m long, 1 to 3 m high, 10 m wide and narrow-crested. It consists of a clast rich to clast supported sandy till, with clasts that are slightly smaller in size compared to those in moraine MB5. Schindelwig et al. (2012) dated four boulders on this moraine (recalculated exposure ages): VBA-17 (10.4 ± 0.5 ka), VBA-18 (10.4 ± 0.6 ka), VBA-19 (10.6 ± 0.5 ka) and VBA-20 (10.8 ± 0.6 ka) (Fig. 5a; Table 2). The probability density function plot shows a unimodal distribution with a tight peak and all samples overlap within internal errors, giving a well-constrained mean age of 10.5 ± 0.3 (0.8) ka.

4.3.2 Luesgenalp valley

At Luesgenalp valley, we distinguished two terminal moraine systems, numbered similarly to those in the Belalp valley in chronological order, from the outermost (morphostratigraphically oldest) to the innermost (morphostratigraphically youngest) (Fig. 7). The first is located to the south of Lengi Egga (Fig. 2), where at least eight glacier advances were identified based on the terminal moraines ML1 to ML8 (Fig. 7). For ML1, ML2 and ML6 the glacier advances are divided in the glacial stages A and B. The second moraine system is south of the artificial lake, where only terminal moraines of four glacier advances (ML-I to ML-IV) were determined (Fig. 7).

To the west of Lengi Egga, there is a right lateral moraine complex, composed of four parallel moraines, numbered 1 through 4 (Fig. 7C). These moraines are, on average, ca. 3 m high, 30 m wide, and narrow-crested. Moraine-1 is the outermost ridge of the complex, extends from 2530 m asl to 2600 m asl and is ca. 250 m long. Moraine-2 can be traced from 2500 m asl to 2595 m asl, where it merges into Moraine-4, and is ca. 340 m long. Moraine-3 is only preserved between 2545 m asl and 2555 m asl, with a length of ca. 60 m. Moraine-4 is the innermost ridge, goes from 2535 m asl to 2625 m asl and is ca. 410 m long. On this right lateral moraine, we collected three samples: LUES-9 (12.3 ± 0.4 ka), LUES-10 (11.4 ± 0.3 ka) and LUES-11 (12.5 ± 0.2 ka) (Table 2). The weighted mean age of this moraine is 12.1 ± 0.3 (1.0) ka.

On the eastern side of Lengi Egga, a well-defined prominent left lateral moraine can be traced for 800 m from ca. 2640 m asl down valley to ca. 2395 m asl, where it ends in the terminal moraine ML1 (Fig. 7). The terminal

moraines ML3 and ML4 separate from this moraine at 2450 m asl and 2530 m asl, respectively. The ridge is up to 15 m high, 90 m wide, and broad to narrow-crested. This moraine is composed of a clast rich sandy till, containing crystalline boulders up to 5 m in length and 2 m in height. We sampled one boulder from this moraine, which yielded an exposure age of 12.9 ± 0.4 ka (LUES-1) (Figs. 6b and 7; Table 2).

Moraine ML1 is the outermost terminal moraine in this valley, marking the maximal extent and the lowest position (ca. 2375 m asl) of the Hostock paleoglacier (Figs. 2, 6 and 7). This ridge is highly disintegrated and largely destroyed by human impact, except for the western end, which is well-preserved (Fig. 7D). ML1 is ca. 1.1 km long, 5 m high, 30 m wide and broad-crested. ML1 bifurcates into two distinct moraines (ML1-A and ML1-B) for ca. 400 m in the southwestern part (Fig. 7).

ML2 is a partially preserved terminal moraine located in the southeast of the Luesgenalp valley (Figs. 6a and 7). This moraine appears in the upper part as a narrow-crested, ca. 1 m high, ca. 10 m wide ridge, that is a few meters to the east of ML1(Fig. 7D). In the lower part, ML2 bifurcates into two ridges (ML2-A and ML2-B) at ca. 2445 m asl (Fig. 7). ML2-A and ML2-B have experienced human impact.

North of ML1 and ML2, ridge ML3 appears as a well-defined terminal moraine (Fig. 7). It extends from the left lateral moraine for 1 km toward west, reaching an elevation of 2530 m asl. MB3 is broad-crested, up to 3 m high and 40 m wide. On this moraine, we sampled four boulders: LUES-2 (12.4 ± 0.4 ka), LUES-3 (12.2 ± 0.8 ka), LUES-4 (11.9 ± 0.7 ka) and LUES-12 (12.0 ± 0.2 ka) (Fig. 6c; Table 2). The probability density function plot shows a unimodal distribution with a tight peak, with a mean age of 12.1 ± 0.2 (0.9) ka for ML3.

Ridge ML4 is a well-constrained and well-preserved terminal and lateral moraine located approximately 100 m north of ML3 (Fig. 7). The ridge is broad-crested, ca. 1100 m long, 25 m wide and 2 to 4 m high. It intercepts the left lateral moraine in the east and ridge ML3 at 2525 m asl in the west, both at a low angle. The moraine is composed of a clast rich sandy till, with crystalline boulders up to the same sizes as those in the left lateral moraine.

Moraines ML5 and ML6 are only partially preserved (Figs. 3 and 7). Moraine ML5 is located a few meters north of ML4, is less than 1 m high and 10 m wide, and broad-crested. Moraine ML6 instead, is 1 m high, 10 m wide and broad-crested. In the central part of the Luesgenalp valley, this moraine appears as two distinct ridges (ML6-A and ML6-B) for ca. 250 m (Fig. 7). For both ML5 and ML6, it was not possible to extrapolate the ridge propagation due to the lack of field evidence.

ML7 is a well-delimited and well-preserved terminal moraine, located ca. 220 m north of ML4 and starting ca. 90 m east of moraine-4 of the right lateral moraine complex, at an altitude of 2540 m asl (Fig. 7). The moraine can be traced as a continuous ridge for 800 m toward the east, reaching the inner side of left lateral moraine at 2550 m asl. ML7 is up to 5 m in height, 30 m in width, and broad to narrow-crested. It is composed of a clast rich sandy till, with boulders up to 2.5 m in length and 1.5 m in height. We collected two boulders on this moraine: LUES-13 (11.2 ± 0.2 ka) and LUES-14 (10.7 ± 0.3 ka) (Table 2). The weighted mean age for moraine ML7 is 11.0 ± 0.2 (0.9) ka.

Moraine ML8 is a well-constrained and well-preserved terminal moraine, situated in the cirque of Lengi Egga and represent the innermost moraine ridge of the moraine system south of Lengi Egga (Figs. 2, 3 and 7). The western end of the moraine dams the stream, forming a pond (Fig. 3). This moraine is ca. 160 m north of ML7, is 530 m long, up to 6 m high, 20 m wide and narrow-crested. It consists of a clast rich sandy till, with clast up to 1.5 m long and 1 m high. Four samples were collected on ML8, yielding exposure ages of 11.6 ± 0.4 ka (LUES-5), 11.7 ± 0.6 ka (LUES-6), 11.5 ± 0.4 ka (LUES-7) and 10.6 ± 0.4 ka (LUES-8) (Table 2). LUES-8 is located on the crest of the moraine; however, the ridge thins vertically in this section, and the surface elevation is approximately 2 m lower than at LUES-7, independent of boulder height. This reduced moraine thickness may have made the boulder more susceptible to exhumation due to surface erosion or sediment reworking (cf. Akçar et al., 2011), thus we exclude LUES-8 from further discussion. The probability density function plot of the three remaining exposure ages shows a unimodal distribution with a tight peak and all samples overlap within their internal errors, obtaining a well-constrained weighted mean age of 11.6 ± 0.3 (0.9) ka for this moraine.

At the artificial lake, the four terminal moraines, ML-I to ML-IV, are between 50 m (ML-IV) and 700 m (ML-I) in length, up to 2.5 m in height, 30 in width and broad-crested (Figs. 3 and 7). The outermost terminal moraine ML-I and moraine ML-III are well-constrained, while the ridges ML-II and ML-IV are only partially preserved. Moraines ML-I and ML-II merge at ca. 2620 m asl and ca. 2630 m asl into the left lateral moraine respectively (Fig. 7).

4.4 Glacier reconstruction

At its maximum extent during the Younger Dryas, the Unnerbaech paleoglacier's margin was located at ca. 2080 m asl and the ELA at 2700 m asl (Fig. 8a). It covered an area of 5 km^2, was 3.9 km in length, and had a thickness of up to 95 m. The accumulation area of the reconstructed glacier was 3.4 km^2 and the ablation area 1.6

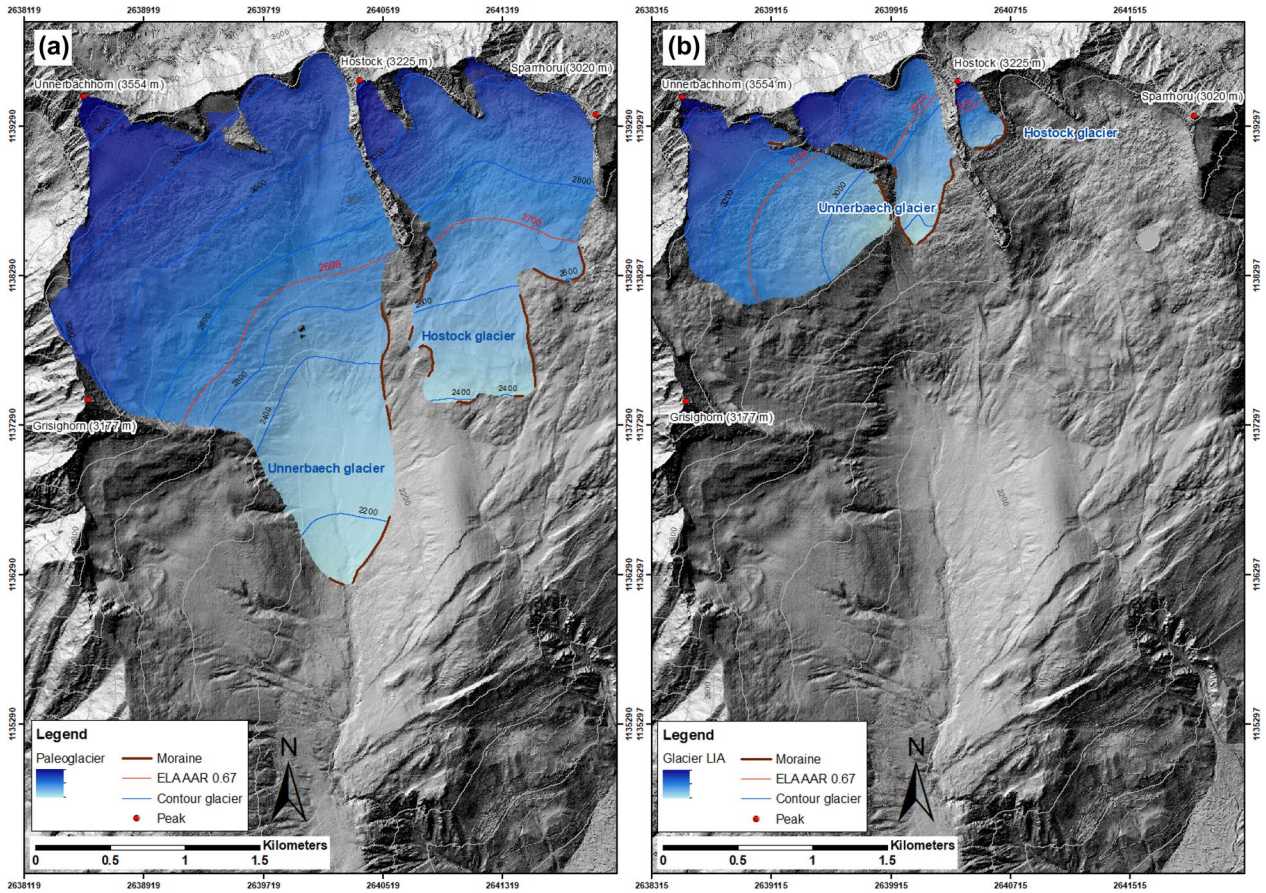

Fig. 8 Reconstructed Unnerbaech and Hostock paleoglaciers in the Belalp and Luesgenalp valleys, respectively. **a** Maximum extent during Younger Dryas. **b** Little Ice Age extent

km^2. During the LIA, the Unnerbaech glacier consisted of two tongues, covering a total area of 1.9 km^2 (Fig. 8b). The first tongue was situated at the Unnerbaechhorn, was 1.6 km long, up to 45 m thick and the ELA was estimated at 3130 m asl. The second tongue was in the eastern part of the Unnerbaech cirque, was 1.2 km in length, up to 50 m in thickness and has an ELA calculated at 3030 m asl (Fig. 8b). We calculated an ELA depression of 330 to 430 m with respect to the LIA ELA, and a corresponding temperature decrease between 2.1 and 2.8 °C for the Unnerbaech paleoglacier at Belalp valley.

The margin of the Hostock paleoglacier was located at ca. 2375 m asl at its maximum extent during the Younger Dryas and we calculated an ELA of 2700 m asl (Fig. 8a). This glacier reached 2.7 km, covered 2.2 km^2, and was up to 80 m thick. It had an accumulation zone of 1.8 km^2 and ablation zone of 0.9 km^2. During the LIA, the Hostock glacier was confined to the northwestern part of the Hostock cirque (Fig. 8b). The glacier covered 0.1 km^2, was 0.5 km in length, up to 40 m in thickness. The ELA is calculated at an altitude of 3100 m asl, resulting in an ELA depression of 400 m relative to the LIA ELA and a temperature decrease of 2.6 °C for the Hostock paleoglacier at Luesgenalp valley.

In addition, to correlate the glacier fluctuations observed at the Belalp and Luesgenalp valleys (Fig. 7) with the paleoclimate proxies, we calculated the paleotemperature for July and the annual paleo-precipitation at the ELA of the maximum glacier extent (Fig. 8a). At an elevation of 2700 m asl a July temperature of 0.8 °C and an annual precipitation interval of 1154–1168 mm/a were archived, based on the quadratic and linear equations described in Ohmura and Boettcher (2018).

5 Discussion

In this study, the paleoglacier reconstructions of Unnerbaech in the Belalp valley and Hostock in the Luesgenalp valley provide critical insights into glacial dynamics during the YD and Early Holocene in the northern Valaisian Alps. By combining high-resolution geomorphological mapping with surface exposure dating, we identified at least eight distinct glacier fluctuations in each valley.

These fluctuations not only capture the maximum extents during the YD but also reflect subsequent readvances in response to Early Holocene climatic oscillations. Our detailed reconstructions extend the existing paleoglaciological record to include tributary valleys that have been underrepresented in previous studies, shedding light on their sensitivity to abrupt climate changes.

The synchrony of glacier advances observed in Belalp and Luesgenalp with other dated YD moraines across the Alps suggests a regionally coherent glacier response to climate cooling, reinforcing the spatial consistency of climatic impacts during the Egesen stadial. This regional contemporaneity, captured through surface exposure dating with cosmogenic ^{10}Be, highlights the robustness of geomorphological evidence for reconstructing glacier fluctuations in tributary valleys. Furthermore, the observed glacier dynamics and ELA depressions not only enhance the understanding of YD climate forcing in the Alps but also provide crucial reference points for improving numerical glacier models. These reconstructions, when integrated with regional climate proxies, offer valuable constraints for calibrating ice-flow simulations and predicting future glacier responses under accelerated warming scenarios. Consequently, our findings underscore the importance of resolving glacier behavior in tributary valleys to better comprehend the full extent of Alpine glaciation and its sensitivity to climate perturbations.

5.1 Glacial geomorphology

The paleoglaciers of Unnerbaech in the Belalp valley and of Hostock in the Luesgenalp valley flowed down to an altitude of 2080 m asl and 2375 m asl respectively and were fed by ice accumulated from the Unnerbaech and Hostock cirques (Fig. 8a). Accordingly, these glaciers oscillated within 3.9 km in the Belalp valley and 2.7 km in the Luesgenalp valley. The ice from the accumulation area of the Unnerbaech paleoglacier was channelized into the U-shaped valley and formed a single glacier tongue in the lower part of the valley (Fig. 8a). This channelization is delineated by glacial landforms (Figs. 3, 5 and 7). Based on the left lateral moraine complex (MB1-7), we estimated a glacier thickness of at least 90 m in the lower part of the valley, which fits well with the thickness of 95 m obtained from our reconstruction. This is consistent with the understanding that a glacier is typically thicker in the central part than at its margins (Baumhauer and Winkler, 2014). In contrast to the U-shaped Belalp valley, Luesgenalp valley is wide and open toward the south (Fig. 2). As a result, the ice from the accumulation area of the Hostock paleoglacier was only partially channelized toward the lower part of the valley. The lateral and terminal moraines mapped in the field provide evidence that this glacier formed two separate tongues (Figs. 3, 7 and 8a).

We suggest that ice from the western and central parts of the cirque fed the tongue south of Lengi Egga, while the ice from the eastern section of the cirque supplied the tongue south of the artificial lake (Fig. 8a). The reconstruction of this paleoglacier yielded a maximum ice thickness of around 80 m at Lengi Egga, which corresponds with the 75 to 80 m expected from our field observation. Overall, the reconstructed glacier extents and thicknesses in the Belalp and Luesgenalp valleys are well-supported by both field evidence and geomorphological mapping, providing robust insights into the glacier dynamics and landscape change during the YD.

5.2 Glacial chronology

5.2.1 Belalp valley

In this study, the formation age of the moraines MB1 and MB2 remains unresolved. The only available age constraint from this moraine system is the boulder VBA-3 (14.8 ± 0.6 ka; recalculated from Schindelwig et al., 2012), located on the left lateral moraine complex MB1-3 (Figs. 5a and 7b). If this exposure age reflects the true timing of deposition—i.e., without influence from nuclide inheritance or reworking—it would suggest that the Unnerbaech glacier must have advanced no later than around 15 ka. However, if the boulder was reworked or contains inherited ^{10}Be concentrations, as its position on the upslope part of the moraine complex MB1–3 might imply, then the moraines MB1 and MB2 could be younger than this age.

Based on the mean surface exposure ages of moraines MB3 (11.8 ± 0.3 ka), MB5 (12.2 ± 0.7 ka), and MB6 (12.1 ± 0.3 ka), we argue that the Unnerbaech paleoglacier advanced during the YD. The timing of MB4 is gauged by the ages of the moraines MB3 and MB5, therefore we conclude that MB4 was also formed during the YD. The obtained moraine chronology in the Belalp valley overlaps within internal errors. Accordingly, we suggest that the glacier advances recorded by the latero-terminal parts of the moraines MB3 to MB6 occurred at around 12 ka.

Moraine MB7 is ca. 400 m up valley from moraine MB6 but still bifurcates from the left lateral moraine complex MB1-7 (Fig. 7). This ridge shows a much smaller glacier extent and size compared to the older moraines MB3 to MB6, despite its similar morphology. We suggest that the Unnerbaech must have retreated at least 400 m before readvancing to form MB7. Afterward, the paleoglacier retreated once again before advancing to deposit MB8 (Fig. 7). This moraine is decoupled from the left lateral moraine complex and lies a few tens of meters further down the slope. Ridge MB8 yields a

well-constrained mean age of 10.5 ± 0.3 ka. Therefore, we suggest that this advance may represent the Unnerbaech glacier's response to the first Early Holocene cooling event, which peaked around 10.4–10.3 ka (Fig. 9) (Le Roy et al., 2024 and references therein). Since then, field evidence suggests that the Unnerbaech paleoglacier retreated to extents smaller than the maximum extent it reached during LIA. In brief, cosmogenic ^{10}Be chronology from the Belalp valley indicate multiple glacial advances during the Younger Dryas, followed by minor re-advances during the Early Holocene, potentially reflecting climatic fluctuations aligned with the first Early Holocene cooling event (Le Roy et al., 2024 and references therein).

5.2.2 Luesgenalp valley

In comparison to the Belalp valley, the glacial chronology in the Luesgenalp valley is much more complex, as it features two terminal moraine systems (ML1 to ML8 and ML-I to ML-IV) and a right lateral moraine complex, each with several distinct ridges (Fig. 7). Moraines ML-I, ML1, Moraine-1 and the left lateral moraine (LLM) mark the maximum glacier extent observed in this valley (Figs. 7 and c). Boulder LUES-1, located on left lateral moraine, yields an exposure age of 12.9 ± 0.4 ka and does not show evidence of being reworked or exhumed (cf. Akçar et al., 2011) (Figs. 3, 6b and 7). Although there was only one boulder available for dating on this moraine (cf. Putkonen and Swanson, 2003), we argue that the Hostock paleoglacier reached it maximal extent no later than around 13 ka. If this boulder does not have any inheritance, this glacier advance may be a response to the Gerzensee Oscillation cold event (GI-1b) (0.4 bis 0.1 ka before YD (Scotti et al., 2017 and references therein) or to the onset of the YD cold phase. The younger moraine ML2 appears only in the southwestern part of the valley as a distinct landform and is located a few tens of meters up valley from ML1 (Fig. 7). This suggests marginal oscillations and similar climatic conditions, presumably of the Early YD.

Based on the mean age of 12.1 ± 0.9 ka for moraine ML3, we propose that this glacial stage belongs to the YD. Given the morphology, geographic position and mean age of 12.1 ± 0.3 ka of Moraine-4 (right lateral moraine complex), we suggest that this ridge is the right lateral continuation of ML3 (Fig. 7). The glacier oscillations recorded by the moraines ML4, ML5, and ML6 have a similar morphology and extent to ML3. This suggests that the glacier fluctuations of ML3 to ML6 occurred under similar climatic conditions and within a short time frame around 12 ka.

The glacier advance recorded by ML7 remains within the left lateral moraine and the right lateral moraine complex, indicating that the glacier no longer occupied the small cirque of Lengi Egga. ML7 provided a mean age of 11.0 ± 0.2 ka, which might correspond to an Early Holocene advance, apparently to the Preboreal Oscillation cold event (e.g. Affolter et al., 2019; Le Roy et al., 2024) (Fig. 9). We calculated a mean age of 11.6 ± 0.3 ka for the younger moraine ML8, which overlaps with the timing of ML7 within uncertainties. Accordingly, we assume that ML8 recorded the last advance of the Hostock paleoglacier at the end of the Younger Dryas, just before the warming at the transition to the Early Holocene. This assumption is aligned with the radiocarbon age from the peat bog at Lengi Egga, which indicates ice free condition no later than ca. 11.4 ka (Tinner and Theurillat, 2003). Afterward, the Hostock paleoglacier must have retreated to extents similar to or smaller than its maximum advance during the LIA. The glacial chronology in the Luesgenalp valley reflects complex glacial dynamics, with distinct advances during the YD and Early Holocene, culminating in ice-free conditions after 11.4 ka.

5.3 Egesen Stadial across the Alps

The boulder exposure ages of the moraines associated with the YD in the Belalp and Luesgenalp valleys overlap all within 2 σ uncertainty, and the paleoglaciers show similar extent (Table 2). To obtain a more consistent age for the glacier advances during the Egesen stadial, we calculated a mean age for the glacier oscillations recorded in the Belalp (12.0 ± 0.9 ka) and Luesgenalp (12.0 ± 1.0 ka) valleys. For Belalp valley we considered all exposure ages belonging to the latero-terminal moraines MB3, MB5, MB6 and of the left lateral moraine complex MB1-7. We excluded the samples VBA-4, VBA-15 due to the reasons mentioned in the results section and VBA-3 because it is about 2 ka older. Samples from moraine MB8 were not included, as the obtained age of 10.5 ± 0.3 (0.8) ka indicate an Early Holocene advance of the Unnerbaech paleoglacier. For Luesgenalp valley, we included all boulder exposure ages from the moraines, as they all belonged to the Egesen stadial. The probability density function analysis detected 3 outliers (LUES-8, LUES-13 and LUES-14), which were excluded. The obtained ages for these two valleys were compared with other dated glacier advances of the Egesen stadial across the Alps dated with cosmogenic nuclides.

With the transition from the warmer interstadial conditions of the Bølling-Allerrød interstadial to the colder stadial conditions at the beginning of the YD, the glaciers across the Alps started to readvance, forming the moraines of the Egesen stadial (Kerschner and Ivy-Ochs, 2008) (Fig. 9). Based on the oldest exposure ages within 2 σ uncertainties of the samples from Belalp and Luesgenalp valleys, glacier expansion likely began around the onset of Younger Dryas cooling, at approximately

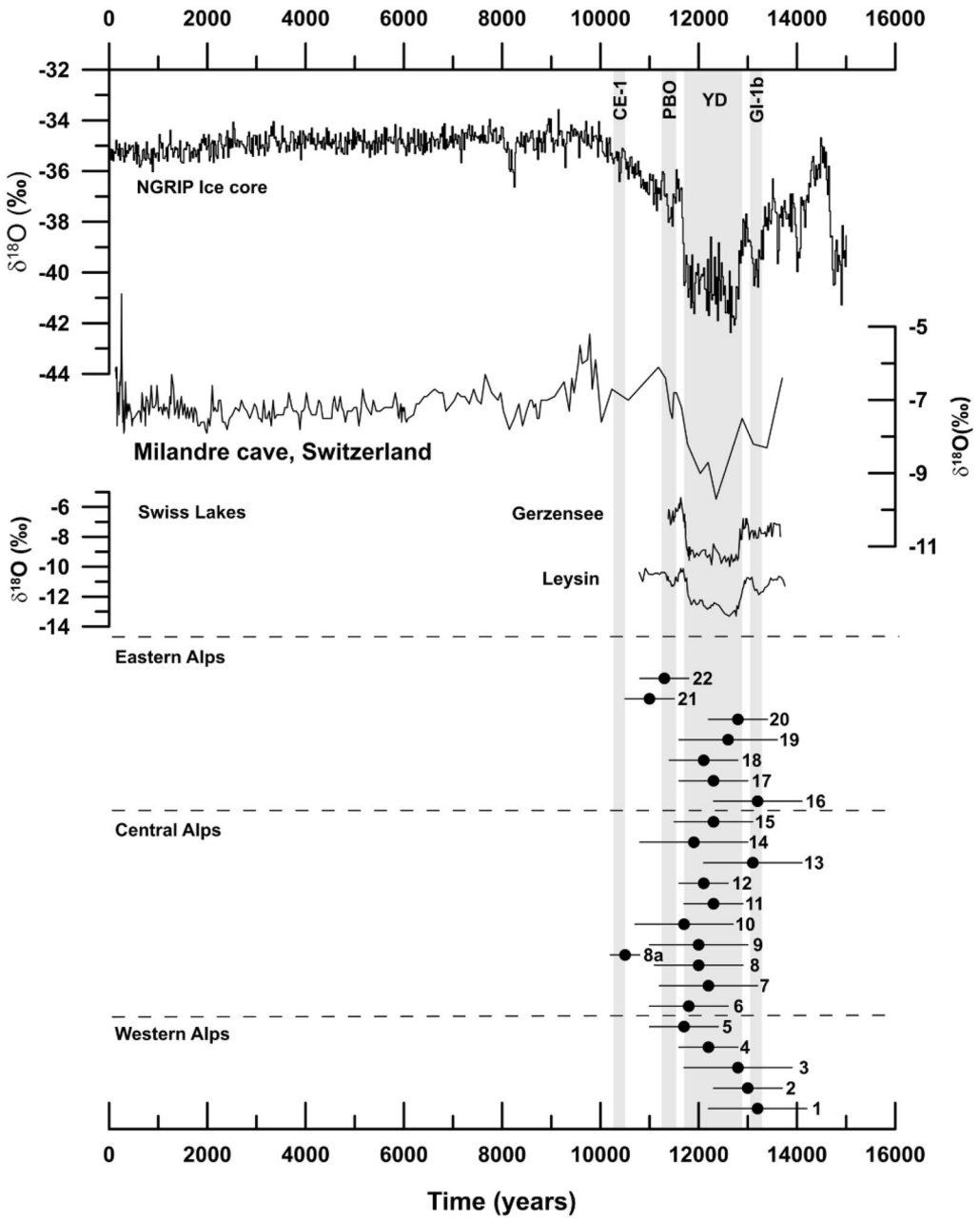

Fig. 9 Comparison of the maximum glacier extent reached by the Unnerbaech and Hostock paleoglaciers and 18 other paleoglaciers in the Alps during the Younger Dryas based on cosmogenic ^{10}Be moraine ages (from Ivy-Ochs et al., 2023). Glacier extents were compared to different climate proxies: NGRIP Ice core in Greenland (Rasmussen et al., 2006); Milandre cave (Affolter et al., 2019) and the lakes Gerzensee and Leysin (Schwander et al., 2000) in Switzerland. The glacier sites are sorted form west (number 1) to east (number 20) and were subdivided into Western, Central and Eastern Alps (after Marazzi, 2005 and references therein). All ages are given with external uncertainties, including the production rate errors (sensu Balco et al., 2008). 1: Gesso valley (Federici et al., 2017); 2: Stura valley (Spagnolo and Ribolini, 2019); 3: Clarée valley (Cossart et al., 2012); 4: Southern Écrins Massif (Hofmann et al., 2019); 5: Mont Blanc Massif (Protin et al., 2019); 6: Grand Paradiso (Baroni et al., 2021); 7: Aletsch (Kelly et al., 2004); 8: Belalp valley (Schindelwig et al., 2012 and this study); 9: Luesgenalp valley (this study); 10: Meien valley (Boxleitner et al., 2019a); 11: Göscheneralp valley (Boxleitner et al., 2019b); 12: Giuv valley (Dieleman et al., 2018); 13: Julier Pass (Ivy-Ochs et al., 2009; Ivy-Ochs, 2015); 14: Mulix valley (Böhlert et al., 2011); 15: Viola valley (Scotti et al., 2017); 16: Schönferwall (Ivy-Ochs et al., 2006); 17: Peio valley (Baroni et al., 2017); 18: Langtaufer valley (Moran et al., 2016); 19: Rauris valley (Bichler et al., 2016); 20: Debant valley (Reitner et al., 2016); 21: Larain valley (Braumann et al., 2021); 22: Jam valley (Braumann et al., 2021). Numbers 1 to 22 of the glaciers in this figure corresponds to numbers of Table 4. Note: number 8a corresponds to the glacier extent of the Unnerbaech paleoglacier in the Belalp valley for moraine MB8

13.1 ± 1.2 ka (VBA-1) and 12.9 ± 1.1 ka (LUES-1). The maximum advance at the Egesen stadial was reached at 12.0 ± 0.9 ka in the Belalp valley and at 12.0 ± 1.0 ka in the Luesgenalp valley (Fig. 9). These data indicate that both paleoglaciers responded in a similar manner to Younger Dryas climate deterioration. The nearby Great Aletsch glacier, with an age of 12.2 ± 1.0 ka (recalculated after Kelly et al., 2004), also reached its maximal extent nearly synchronously with the paleoglaciers in the tributary valleys of Belalp and Luesgenalp (Fig. 9). This suggests similar climatic conditions for the northern Valaisian Alps.

The maximum extent of the northern Valaisian Alps was nearly synchronous with the Rougnoux paleoglacier of the southern Écrins Massif (12.2 ± 0.6 ka; Hofmann et al., 2019) in the Western Alps; with the paleoglacier of the Göscheneralp valley (12.3 ± 0.6 ka; Boxleitner et al., 2019b) in the Bernese Alps; with the Giuv paleoglacier (12.1 ± 0.5 ka; Dieleman et al., 2018) in the Glarus Alps; with the Mulix valley paleoglacier (11.9 ± 1.1 ka; Böhlert et al., 2011) and the Dosdè paleoglacier of Viola valley (12.3 ± 0.8 ka; Scotti et al., 2017) in the western Rhaetian Alps, with the La Mare paleoglacier of the Peio valley (12.3 ± 0.7 ka; Baroni et al., 2017) in the southern Rhaetian Alps; and with the Langtaufer valley paleoglacier (12.1 ± 0.7 ka; Moran et al., 2016) in the eastern Rhaetian Alps (Fig. 9; Table 4). They are earlier than that of the Argentieré paleoglacier (11.7 ± 0.7 ka; Protin et al., 2019) in the Pennine Alps; the paleoglaciers at Grand Paradiso (11.8 ± 0.8 ka; Baroni et al., 2021) in the Graian Alps; and the Meien valley paleoglacier (11.7 ± 1.0 ka; Boxleitner et al., 2019a) in the Bernese Alps (Fig. 9; Table 4). The paleoglacier in the Gesso valley (13.2 ± 1.0 ka Federici et al., 2017); and the Forneris paleoglacier in the Stura valley (13.0 ± 0.7 ka; Spagnolo and Ribolini, 2019) in the Maritime Alps; the Clarée paleoglacier (12.8 ± 1.1 ka; Cossart et al., 2012) in the Western Alps; the Vadret paleoglacier at Julier Pass (13.1 ± 1.0 ka; Ivy-Ochs et al., 2009; Ivy-Ochs, 2015) and the Schönferwall paleoglacier (13.2 ± 0.9 ka; Ivy-Ochs et al., 2006) in the western Rhaetian Alps, and the paleoglacier in the Rauris valley (12.6 ± 1.0 ka; Bichler et al., 2016) and Debant paleoglacier in the Debant valley (12.8 ± 0.6 ka; Reitner et al., 2016) in the western Tauern Alps, instead reached the maximum extent earlier than the northern Valaisian Alps glaciers (Fig. 9 and Table 4). Therefore, the maximum advance of Alpine glaciers ranges from 13.2 ± 1.0 ka for the paleoglacier in the Gesso valley (Federici et al., 2017) to 11.7 ± 1.0 ka for the paleoglacier in the Meien valley (Boxleitner et al., 2019b), indicating a broad scatter of timing that covers the entire YD. Some glaciers appear to have reached their maximum positions as early as the beginning of the YD (e.g., Debant and Clarée paleoglaciers) or perhaps even earlier (e.g., Schönferwall paleoglacier and the paleoglacier in the Gesso valley). This suggests that climate conditions favorable for glacier advances may have occurred already before the YD cold phase, possibly during the cold event of the Gerzensee Oscillation (GI-1b), as recorded by the NGRIP ice core (Rasmussen et al., 2006), the Milandre cave in Switzerland (Affolter et al., 2019) and the Swiss lakes of Gerzensee and Leysin (Schwander et al., 2000) (Fig. 9).

The Alpine glaciers reached their maximum extent during the Egesen stadial at approximately 12.4 ± 0.8 ka. This age corresponds to the arithmetic average of the 20 exposure dated sites given in Fig. 9. The timing of the maximum extent of the Egesen glaciers appears to be broadly synchronous across the Alps, within the uncertainties of existing exposure ages. In the Western Alps, the maximum advance occurred at around 12.8 ± 0.9 ka, and in the Eastern Alps, it was around 12.5 ± 0.9 ka. The central Alpine glaciers reached their maximum advance at approximately 12.0 ± 0.8 ka (Fig. 9). These ages represent the arithmetic average of the maximum glacier positions in each region.

The Unnerbaech and Hostock paleoglaciers in the study area extended down to an altitude of ca. 2080 m asl and ca. 2375 m asl, respectively, corresponding to the fifth highest and the highest values observed in the Alps during the YD (Table 4). In contrast, the glacier that descended the most was the nearby Great Aletsch glacier, reaching an altitude of around 700 m asl (Kelly et al., 2004). This resulted in an elevation difference of approximately 1700 m over just a few kilometers. The minimum altitude reached by the Alpine glaciers at their maximum extent varied mainly within 1700 m asl and 2100 m asl (Table 4). Larger glaciers generally descended to lower elevations (e.g. Argentieré glacier at 1200 m asl; Protin et al., 2019) compared to smaller glaciers (e.g. Forneris paleoglacier at ca. 1900 m asl; Spagnolo and Ribolini, 2019). This can be attributed to the significant difference in size and the larger accumulation area between extensive valley glaciers and smaller cirque glaciers. In addition, glaciers facing northwest, north and northeast reached, on average, lower elevations than those facing west, south and east, with altitudes of ca. 1680 m asl compared to 1850 m asl, respectively (Table 4). Our chronology from the Belalp and Luesgenalp valleys support the interpretation that the glacier maxima during the Egesen stadial were broadly synchronous across the Alps, reinforcing the regional climatic influence of the Younger Dryas on glacier dynamics (cf. Ivy-Ochs et al., 2023). Furthermore, our results extend this understanding to tributary valleys in the northern Valaisian Alps, which have been previously underrepresented in regional glacial chronologies.

Table 3 Characteristics of the reconstucted glaciers at Belalp and Luesgenalp valleys

Location (valley)	Glacier	Length YD (km)	Area YD (km^2)	YD ELA estimate (m asl) AAR value 0.5	0.6	0.67	0.8	Length LIA (km)	Area LIA (km^2)	LIA ELA estimate (m asl) AAR value 0.67	ΔELA (m)	ΔT (°C)
Belalp	Unnerbaech	3.9	5	2900	2800	2700	2500	1.2–1.6	1.9	3030–3130	430–330	2.1–2.8
Luesgenalp	Hostock	2.7	2.2	2800	2750	2700	2650	0.5	0.1	3100	400	2.6

Reported glacier length for the Younger Dryas corresponds to the maximum extent of the both paleoglaciers during this period, based on the outermost preserved moraine ridge

Table 4 *Summary of the glacier extents of 20 paleoglaciers dated with cosmogenic ^{10}Be (adapted from* Ivy-Ochs et al., 2023)

Nr	Study area	Alpine section	Facing of the glaciers	Age (ka)	Minimum altitude at the maximum extent (m asl)	ELA at the maximum extent (m asl)	ELA depression (m)	References
1	Gesso valley	Western Alps	North	13.2 ± 1.0	1800	2335 (AABR)	473	Federici et al. (2017)
2	Stura valley	Western Alps	North	13.0 ± 0.7	1900	2349 (AABR)	–	Spagnolo and Ribolini (2019)
3	Clarée valley	Western Alps	Southeast	12.8 ± 1.1	1900	2427 (AABR)	450	Cossart et al. (2012)
4	Southern Écrins Massif	Western Alps	Northwest	12.2 ± 0.6	1880	2218 (AAR)	226	Hofmann et al. (2019)
5	Mont Blanc Massif	Central Alps	Northwest	11.7 ± 0.7	1200	2523 (AABR)	215	Protin et al. (2019)
6	Grand Paradiso*	Central Alps	North	11.8 ± 0.8	1685	2764 (AAR)	231	Baroni et al. (2021)
7	Aletsch	Central Alps	Southeast	12.2 ± 1.0	700	–	–	Kelly et al. (2004)
8	Belalp valley	Central Alps	South	12.0 ± 0.9	2080	2700 (AAR)	330–430	Schindelwig et al. (2012); this study
9	Luesgenalp valley	Central Alps	South	12.0 ± 1.0	2375	2700 (AAR)	400	This study
10	Meien valley	Central Alps	Northeast	11.7 ± 1.0	1260	2235 (AAR)	285	Boxleitner et al., 2019a
11	Göscheneralp valley	Central Alps	Northeast	12.3 ± 0.6	1150	2110 (AAR)	435	Boxleitner et al., 2019b
12	Val Giuv	Central Alps	South	12.1 ± 0.5	1700	2300 (AAR)	400	Dieleman et al., 2018
13	Julier Pass	Eastern Alps	North	13.1 ± 1.0	2180	2525 (AAR)	220	Ivy-Ochs et al. (2009)
14	Mulix valley	Eastern Alps	North	11.9 ± 1.1	1950	2499 (AAR)	–	Böhlert et al. (2011)
15	Viola valley	Eastern Alps	North	12.3 ± 0.8	2100	2650 (AAR)	220	Scotti et al. (2017)
16	Schönferwall	Eastern Alps	North	13.2 ± 0.9	1700	2320 (AAR)	290	Ivy-Ochs et al. (2006)
17	Peio valley	Eastern Alps	Southeast	12.3 ± 0.7	2000	2845 (AAR)	225	Baroni et al. (2017)
18	Langtaufer valley	Eastern Alps	West	12.1 ± 0.7	2300	2650 (AAR)	220	Moran et al. (2016)
19	Rauris valley	Eastern Alps	North	12.6 ± 1.0	1300	2234 (AABR)	–	Bichler et al. (2016)
20	Debant valley	Eastern Alps	Southwest	12.8 ± 0.6	1730	2520 (AAR)	–	Reitner et al. (2016)
21	Larain valley	Eastern Alps	North	11.0 ± 0.5	2160	–	–	Brauman et al. (2021)
22	Jam valley	Eastern Alps	North	11.3 ± 0.5	–	–	–	Brauman et al. (2021)

* Mean age of all paleoglaciers at Grand Paradiso

The reported ELAs of paleoglaciers at the maximum extent during the YD varied by approximately 750 m across the Alps (Table 4). For both the Unnerbaech and Hostock paleoglaciers in the Belalp and Luesgenalp valleys, an ELA of 2700 m asl was calculated (Fig. 8). The ELAs in the study area were among the

highest determined for the Egesen stadial in the Alps. Only the calculated ELAs of the La Mare paleoglacier in the Peio valley (2845 m asl, AAR 0.67; Baroni et al., 2017) and the Paleoglaciers at Grand Paradiso (2764 m asl, AAR 0.67; Baroni et al., 2021) were higher. The lowest ELAs were determined for the Göscheneralp paleoglacier (2110 m asl, AAR 0.67; Boxleitner et al., 2019a), the paleoglacier in the Meien valley (2235 m asl with AAR 0.67; Boxleitner et al., 2019a), Rougnoux paleoglacier in the Clarée valley (2218 m asl, AAR 0.67; Hofmann et al., 2019) and the paleoglacier at Rauris valley (2234 m asl, AABR method; Bichler et al., 2016).

We observed that paleoglaciers located in the interior valleys of the Central and Eastern Alps generally had higher ELAs than those in the northern fringe. In addition, paleoglaciers facing northwest, north and northeast had, on average, lower ELAs than those oriented west, south and east (approximately 2400 m asl versus 2600 m asl respectively). This implies that valley orientation influenced ELA elevation and presumably also the formation of the paleoglacier. In fact, more than the half of the Paleoglaciers during the YD developed primarily on slopes facing northwest, north and northeast (Table 4).

The ELA depression calculated between the maximum extent of the Unnerbaech and Hostock paleoglaciers during the Egesen stadial and the LIA maximum was 330–430 m and 400 m, respectively (Fig. 8, Table 3 and 4). Our results align with the reported range of YD ELA depressions for the Alps, which is between 180 and 450 m, as reported by Kerschner et al. (2000) and Kerschner and Ivy-Ochs (2008). Similarly high values, like those in our study area, have been observed along the northern fringe of the Alps, the Western Alps and the Maritime Alps. Examples include i.e. the Giuv paleoglacier with 400 m (Dieleman et al., 2018); the Göscheneralp paleoglacier with 435 m (Boxleitner et al., 2019b); the Clarée paleoglacier with 450 m (Cossart et al., 2012); and the Gesso valley paleoglacier with 473 m (Federici et al., 2017) (Table 4). These findings are consistent with the studies by Kerschner and Ivy-Ochs (2008) and Cossart et al., (2012). In contrast, significantly lower ELA depression values were mainly observed in the interior Alpine valleys. For instance, the Grand Paradiso paleoglacier had a depression of 231 m (Baroni et al., 2021); the Argentieré paleoglacier 215 m (Protin et al., 2019), the Vadret Lagrev paleoglacier 220 m (Ivy-Ochs et al., 2009; Ivy-Ochs, 2015); and La Mare paleoglacier 225 m (Baroni et al., 2017) (Table 4). ELA depressions in the interior valleys of the Alps typically ranged from 200 to 250 m (Kerschner and Ivy-Ochs, 2008).

5.4 Paleoclimate and climatic drivers in the Northern Valaisian Alps during the YD

The position of the ELA over time of a glacier is closely related to the climatic parameters, particularly temperature and precipitation, of the area under investigation, providing relevant paleoclimatic information in this regard (Baroni et al., 2021). With an ELA depression of 330 m to 430 m at the Unnerbaech paleoglacier and 400 m at the Hostock paleoglacier, and assuming a standard lapse rate of 0.65 °C per 100 m, we estimated an temperature depression of 2.1 to 2.8 °C in the Belalp valley and 2.6 °C in the Luesgenalp valley, compared to LIA conditions. This indicates a significant temperature drop during the YD, which is also recorded in the $\delta^{18}O$ curves of the NGRIP ice core (Rasmussen et al., 2006), the Milandre cave in Switzerland (Affolter et al., 2019) and the Swiss lakes of Gerzensee and Leysin (Schwander et al., 2000) (Fig. 9). Our findings are consistent with chironomid-based summer temperature reconstructions across the Alpine region, which suggest a temperature depression in the Alps in the order of 3.5 °C (Heiri et al., 2014 and references therein).

The reconstructed temperature depression during the YD in the broader European region, including the Alps, has been extensively investigated using both climate models and various proxy-based reconstructions (cf. Renssen et al., 2018). Chironomid-based temperature reconstructions indicate significant cooling across Europe during the YD, with estimates ranging from 2–4° C, primarily driven by the weakening of the Atlantic Meridional Overturning Circulation. In the Swiss Jura, pollen and lake-level data suggest climatic instability during the YD, marked by episodes of drying and intermittent summer warming (Magny et al., 2001). Multi-proxy studies in the Alps, which incorporate both pollen and chironomid assemblages, estimate temperature reductions of about 2–3° C during the YD, with mean summer temperatures dropping to 9–10° C, consistent with glacial evidence from ELA reconstructions (Lotter et al., 2000; Heiri et al., 2014).

Our findings compare well with climate modeling efforts that simulate pronounced cooling patterns across Europe during the YD, driven by shifts in atmospheric circulation and temperature anomalies (e.g., Isarin and Renssen, 1999). Although these models often focus on broader European perspectives, they support the general trend of significant cooling during this period, which is consistent with our findings from the Belalp and Luesgenalp valleys. Further validation of these temperature depressions is found in pollen-based reconstructions from Western Europe, where multi-proxy records indicate climatic fluctuations, including a two-phase pattern of wetter and drier conditions rather than uniformly

cooler temperatures (Hepp et al., 2019). High-resolution pollen-based records from the Alps confirm correlations with broader North Atlantic climate signals during the YD, although specific magnitudes of temperature changes are not always explicitly detailed (Pini et al., 2022). Elevational transects of modern pollen samples in the Alps have provided valuable calibration for reconstructing past climatic shifts (Furlanetto et al., 2019). While these studies do not directly quantify YD cooling, they validate the reliability of pollen-based temperature reconstructions in the region. Moreover, Rea et al. (2020) combined multi-proxy records to model atmospheric circulation over Europe, demonstrating widespread temperature drops consistent with our estimates for the northern Valaisian Alps.

Collectively, these reconstructions confirm that the 2.1–2.8° C temperature depression inferred from ELA shifts in the Belalp and Luesgenalp valleys aligns well with the broader European paleoclimate context. This consistency across different proxies and modeling approaches strengthens the argument for a significant YD cooling phase in the Alpine region, well-integrated within the European climate framework. The agreement between our ELA-based temperature estimates and independent pollen-based and modeling studies supports the robustness of our reconstructed glacier extents.

The annual paleo-precipitation at the ELA, estimated from chironomid assemblages at Lago Piccolo di Avigliana in Italy (Larocque and Finsinger, 2008), ranged between 1154 mm/a and 1168 mm/a for the study area, based on P/T equations described by Ohmura and Boettcher (2018). These values align with the annual paleo-precipitation of 1060 mm/a to 1230 mm/a estimated using the independent model PaleoClim (Fordham et al., 2017; Karger et al., 2017; Brown et al., 2018) (Fig. 10a). In contrast, Rea et al., (2020) suggested drier

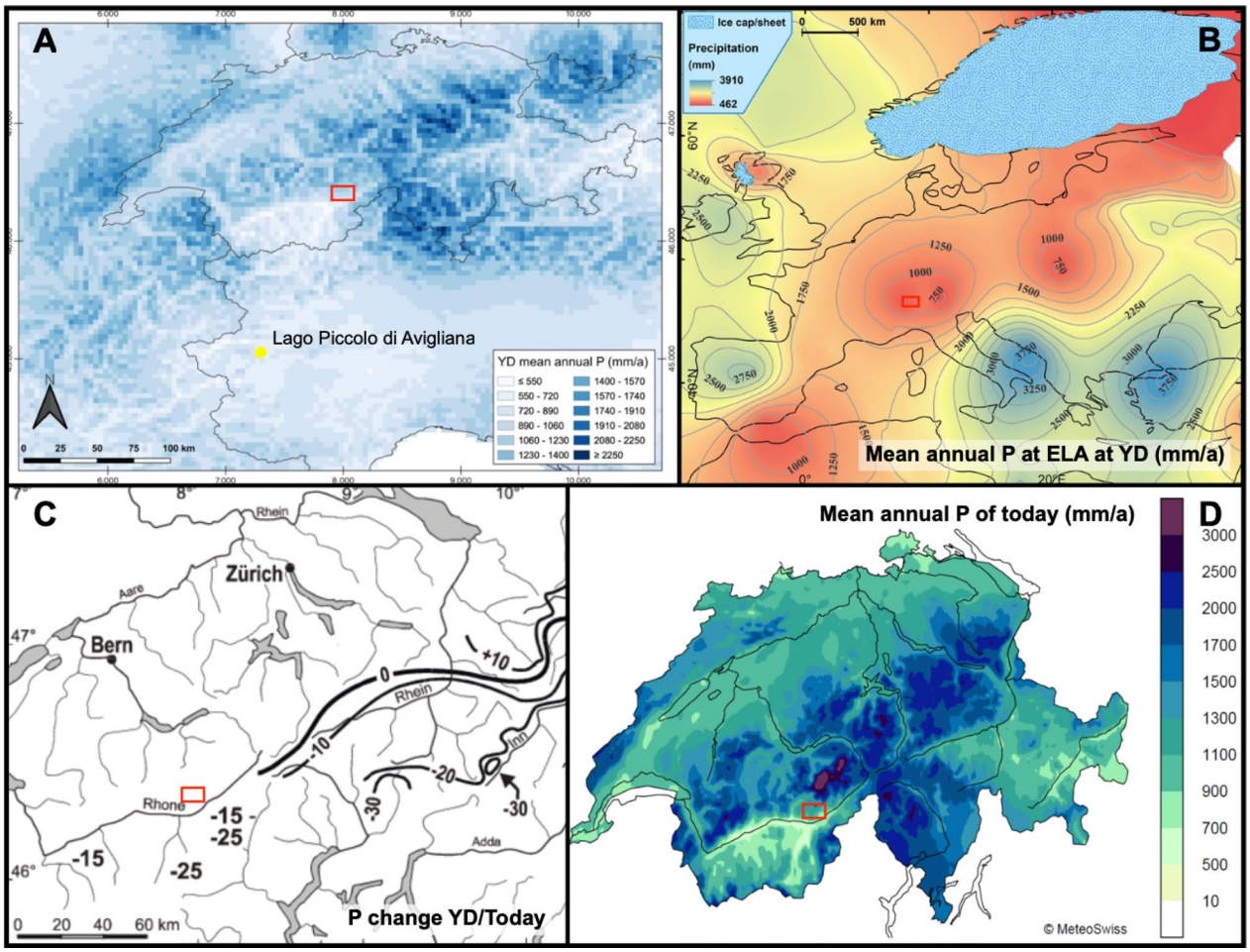

Fig. 10 **A** distribution of the paleo-precipitations (mm/a) modeled for the YD from PaleoClim (Fordham et al., 2017; Karger et al., 2017; Brown et al., 2018). **B** Mean annual precipitation at the ELA (mm/a) estimated by Rea et al., (2020). **C** Precipitation change between Younger Dryas and Little Ice Age presented by Kerschner et al., (2000). **D** Annual precipitation (mm/a) for the period 1991–2020 in Switzerland (©MeteoSwiss). Red rectangles illustrate the position of the study area

conditions for the northern Valaisian Alps, with precipitation amounts of less than 1000 mm/a (Fig. 10b). This discrepancy might be due to the limited availability of site-specific paleo-precipitation data across the Alps (Protin et al., 2019).

According to Kerschner et al. (2000) (Fig. 10c), the interior valleys experienced a reduction in rainfall of up to 30% compared to present-day values, while the northern fringe saw an increase of up to 10%. This shift in precipitation patterns was likely due to dominant western to northwestern atmospheric circulations, which brought more humid air toward the northern fringe the Maritime and Western Alps, but less toward the interior valleys of the Central and Eastern Alps (e.g. Federici et al., 2008; Kerschner and Ivy-Ochs, 2008; Cossart et al., 2012).

For the northern Valaisian Alps, which are located in an interior valley, no significant trend in the precipitation pattern was detected, suggesting conditions similar but cooler to those of the present-day. This is supported by the annual total precipitation data for the period 1991–2020 in Switzerland (©MeteoSwiss), where precipitation at the paleo-ELA of the study area ranged within 1100 mm and 1300 mm (Fig. 10d). We assume that the precipitation pattern during the YD and the present day are comparable, indicating similar conditions over the last 13 ka. Analogous results were observed at the Grand Paradiso (Baroni et al., 2021). Our findings underscore the dominant role of temperature depression in driving glacier advances during the YD in the northern Valaisian Alps, highlighting the sensitivity of local glaciers to abrupt cooling events rather than changes in moisture availability. By reconstructing multiple advances of the small tributary glaciers in the Belalp and Luesgenalp valleys, we provide a highly detailed record of glacier fluctuations during the Younger Dryas. While the Great Aletsch Glacier also responded to Younger Dryas climate fluctuations, its preserved moraine record is less pronounced (cf. Kelly et al., 2004). This comparison highlights how small, confined glacier systems can archive a finer sequence of climate-driven advances, offering valuable insights into regional glacier–climate interactions during the last deglaciation.

6 Conclusions

In this study, we investigated the Lateglacial and Early Holocene glacier fluctuations in the Belalp and Luesgenalp valleys, focusing on the reconstruction of glaciers extents based of the moraine systems present at the study area (Figs. 3, 4, and 5). Field evidence indicates at least eight glacier advances at both study sites: MB1-MB8 in the Belalp valley and ML1-ML8 in the Luesgenalp valley (Fig. 7). The paleoglaicers of Unnerbaech and Hostock began to expand before 13.1 ± 1.2 ka (VBA-1) and 12.9 ± 1.1 ka (LUES-1) respectively, with the onset of the YD (Fig. 7). The maximum advance during the Egesen stadial was reached at 12.0 ± 0.9 ka in the Belalp valley and 12.0 ± 1.0 ka in the Luesgenalp valley (Fig. 9). The timing of the maximum glacier advances in our study area aligns well with the timing of the Egesen stadial in the Alps, within the uncertainties (Fig. 9).

At their maximum extent, the Unnerbaech paleoglacier reached 3.9 km in length and covered 5 km^2, while the Hostock paleoglacier reached 2.7 km in length and covered 2.2 km^2 (Fig. 8). An ELA of 2700 m asl was determined for the YD, with ELA depressions relative to the LIA ELA estimated to be between 330 and 430 m in the Belalp valley and 400 m in the Luesgenalp valley. These ELA depressions correspond to temperature decrease of 2.1 to 2.8 °C compared to LIA conditions. In addition, paleo-precipitation reconstructions suggest that precipitation pattern during the YD were similar to those of the present-day for the study area. This research contributes to a broader understanding of glacier evolution in the Alps during the YD cold phase and provides further insights into the paleoclimate of the Alps on both local and regional scales by reconstructing paleotemperature and precipitation in the Belalp and Luesgenalp valleys.

Acknowledgements
We sincerely thank Dr. Vjeran Višnjević from the University of Bern and the anonymous reviewer for their positive and constructive comments, which greatly contributed to improving our manuscript during the revision process. Special thanks go to Julijana Gajic for her assistance with laboratory introduction and sample preparation at the Institute of Geological Sciences, University of Bern. We would like to extend our gratitude to Catharina Dieleman for her support during the introduction to glacier reconstruction. Furthermore, we appreciate the analyses conducted at the Zürich AMS Facility operated by the Swiss Federal Institute of Technology (ETH Zürich), Switzerland. This study is financed by the Glacial Geology Group at the Institute of Geological Sciences, University of Bern. We are also grateful to CH-QUAT for the financial support during the fieldwork.

Author contributions
N.A., S.I.O., and C.S. designed the study. M.B. and N.A. completed the field work including, mapping, taking the areal images, and sampling. M.B. prepared the samples for the AMS analysis of cosmogenic ^{10}Be. M.C. performed the AMS measurements. M.B. and S.Y. completed the photogrammetric analysis of aerial images and reconstructed the paleoglaciers. M.B. wrote the manuscript and prepared the figure and tables. All authors contributed to the manuscript.

Funding
This study is financed by the Glacial Geology Group at the Institute of Geological Sciences, University of Bern. We are also grateful to CH-QUAT for the financial support during the fieldwork.

Data availability
No datasets were generated or analysed during the current study.

Declarations

Competing interests
The authors declare no competing interests.

Received: 17 January 2025 Accepted: 16 June 2025
Published online: 05 September 2025

References

Affolter, S., Häuselmann, A., Fleitmann, D., Edwards, R. L., Cheng, H., & Leuenberger, M. (2019). Central Europe temperature constrained by speleothem fluid inclusion water isotopes over the past 14,000 years. *Science Advances, 5*(6), 3809. https://doi.org/10.1126/sciadv.aav3809

Agisoft (2014) 'Tutorial (beginner level): Orthophoto and DEM generation with Agisoft PhotoScan Pro 1.1 (with ground controls points)', 1.

Agisoft (2017) 'Tutorial (Beginner level): Orthomosaic and DEM Generation with Agisoft PhotoScan Pro 1.2 (without Ground Control Points)', 2, pp. 1–14. https://doi.org/10.1006/mpev.1996.0003.

Akçar, N., Deline, P., Ivy-Ochs, S., Alfimov, V., Hajdas, I., Kubik, P. W., Christl, M., & Schlüchter, C. (2012). The AD 1717 rock avalanche deposits in the upper Ferret Valley (Italy): A dating approach with cosmogenic 10Be. *Journal of Quaternary Science, 27*(4), 383–392. https://doi.org/10.1002/jqs.1558

Akçar, N., Ivy-Ochs, S., Alfimov, V., Schlunegger, F., Claude, A., Reber, R., Christl, M., Vockenhuber, C., Dehnert, A., Rahn, M., & Schlüchter, C. (2017). Isochron-burial dating of glaciofluvial deposits: First results from the Swiss Alps. *Earth Surface Processes and Landforms, 42*(14), 2414–2425. https://doi.org/10.1002/esp.4201

Akçar, N., Ivy-Ochs, S., Kubik, P. W., & Schlüchter, C. (2011). Post-depositional impacts on "Findlinge" (erratic boulders) and their implications for surface-exposure dating. *Swiss Journal of Geosciences, 104*(3), 445–453. https://doi.org/10.1007/s00015-011-0088-7

Akçar, N., Yavuz, V., Ivy-Ochs, S., Kubik, P. W., Vardar, M., & Schlüchter, C. (2007). Cosmogenic exposure dating of snow-avalanche ridges Eastern Black Sea Mountains, NE Turkey. *Quaternary International, 167*, 4–11. https://doi.org/10.1016/j.quaint.2006.11.011

Alley, R. B. (2000). The Younger Dryas cold interval as viewed from central Greenland. *Quaternary Science Reviews, 19*(1–5), 213–226. https://doi.org/10.1016/S0277-3791(99)00062-1

Alley, R. B., & Clark, P. U. (1999). The deglaciation of the northern hemisphere: A global perspective: A Global Perspective. *Annual Review of Earth and Planetary Sciences, 27*, 149–182. https://doi.org/10.1146/annurev.earth.27.1.149

Andre, M. F. (2002). Rates of postglacial rock weathering on glacially scoured outcrops (Abisko-Riksgransen area, 68 degrees N). *Geografiska Annaler Series A-Physical Geography, 84A*(3–4), 139–150. https://doi.org/10.1111/j.0435-3676.2002.00168.x

Bakke, J., Lie, O., Heegaard, E., Dokken, T., Haug, G. H., Birks, H. H., Dulski, P., & Nilsen, T. (2009). Rapid oceanic and atmospheric changes during the Younger Dryas cold period. *Nature Geoscience, 2*(3), 202–205. https://doi.org/10.1038/Ngeo439

Balco, G., Stone, J. O., Lifton, N. A., & Dunai, T. J. (2008). A complete and easily accessible means of calculating surface exposure ages or erosion rates from Be-10 and Al-26 measurements. *Quaternary Geochronology, 3*(3), 174–195. https://doi.org/10.1016/j.quageo.2007.12.001

Baroni, C., Casale, S., Salvatore, M. C., Ivy-Ochs, S., Christl, M., Carturan, L., Seppi, R., & Carton, A. (2017). Double response of glaciers in the Upper Peio Valley (Rhaetian Alps, Italy) to the Younger Dryas climatic deterioration. *Boreas, 46*(4), 783–798. https://doi.org/10.1111/bor.12284

Baroni, C., Gennaro, S., Salvatore, M. C., Ivy-Ochs, S., Christl, M., Cerrato, R., & Orombelli, G. (2021). Last Lateglacial glacier advance in the Gran Paradiso Group reveals relatively drier climatic conditions established in the Western Alps since at least the Younger Dryas. *Quaternary Science Reviews, 255*, Article 106815. https://doi.org/10.1016/j.quascirev.2021.106815

Baumhauer, R. W., S. (2014). *Glazialgeomorphologie*. Schweizerbart Science Publishers. Available at: http://www.schweizerbart.de//publications/detail/ isbn/9783443071516/Baumhauer_Winkler_Glazialgeomorphologie.

Berger, A., Mercolli, I., Herwegh, M., Gnos, E. (2017). Geological Map of the Aar Massif, Tavetsch and Gotthard Nappes. *Geological Special Map 1:100'000, Explanatory Notes 129*.

Bichler, M. G., Reindl, M., Reitner, J. M., Drescher-Schneider, R., Wirsig, C., Christl, M., Hajdas, I., & Ivy-Ochs, S. (2016). Landslide deposits as stratigraphical markers for a sequence-based glacial stratigraphy: A case study of a Younger Dryas system in the Eastern Alps. *Boreas, 45*(3), 537–551. https://doi.org/10.1111/bor.12173

Böhlert, R., Egli, M., Maisch, M., Brandová, D., Ivy-Ochs, S., Kubik, P. W., & Haeberli, W. (2011). Application of a combination of dating techniques to reconstruct the Lateglacial and early Holocene landscape history of the Albula region (eastern Switzerland). *Geomorphology, 127*(1), 1–13. https://doi.org/10.1016/j.geomorph.2010.10.034

Boxleitner, M., Ivy-Ochs, S., Egli, M., Brandova, D., Christl, M., & Maisch, M. (2019a). Lateglacial and Early Holocene glacier stages - New dating evidence from the Meiental in central Switzerland. *Geomorphology, 340*, 15–31. https://doi.org/10.1016/j.geomorph.2019.04.004

Boxleitner, M., Ivy-Ochs, S., Egli, M., Brandova, D., Christl, M., Dahms, D., & Maisch, M. (2019b). The 10Be deglaciation chronology of the Göschenertal, central Swiss Alps, and new insights into the Göschenen Cold Phases. *Boreas, 48*(4), 867–878. https://doi.org/10.1111/bor.12394

Braumann, S. M., Schaefer, J. M., Neuhuber, S. M., Lüthgens, C., Hidy, A. J., & Fiebig, M. (2021). Early Holocene cold snaps and their expression in the moraine record of the eastern European Alps. *Clim. past, 17*(6), 2451–2479. https://doi.org/10.5194/cp-17-2451-2021

Brown, J. L., Hill, D. J., Dolan, A. M., Carnaval, A. C., & Haywood, A. M. (2018). PaleoClim, high spatial resolution paleoclimate surfaces for global land areas. *Scientific Data, 5*(1), Article 180254. https://doi.org/10.1038/sdata.2018.254

Chandler, B. M. P., Lovell, H., Boston, C. M., Lukas, S., Barr, I. D., Benediktsson, Í. Ö., Benn, D. I., Clark, C. D., Darvill, C. M., Evans, D. J. A., Ewertowski, M. W., Loibl, D., Margold, M., Otto, J.-C., Roberts, D. H., Stokes, C. R., Storrar, R. D., & Stroeven, A. P. (2018). Glacial geomorphological mapping: A review of approaches and frameworks for best practice. *Earth-Science Reviews, 185*, 806–846. https://doi.org/10.1016/j.earscirev.2018.07.015

Chiba, T., Kaneta, S.-I., & Suzuki, Y. (2008). Red relief image map: New visualization method for three dimensional data. *The International Archives of the Photogrammetry, Remote Sensing and Spatial Information Sciences, 37*, 1071–1076.

Chmeleff, J., von Blanckenburg, F., Kossert, K., & Jakob, D. (2010). Determination of the Be-10 half-life by multicollector ICP-MS and liquid scintillation counting. *Nuclear Instruments & Methods in Physics Research Section B-Beam Interactions with Materials and Atoms, 268*(2), 192–199. https://doi.org/10.1016/j.nimb.2009.09.012

Christl, M., & Kubik, P. W. (2013). New Be-cathode preparation method for the ETH 6 MV Tandem. *Nuclear Instruments & Methods in Physics Research Section B-Beam Interactions with Materials and Atoms, 294*, 199–202. https://doi.org/10.1016/j.nimb.2012.03.004

Cossart, E., Fort, M., Bourlès, D., Braucher, R., Perrier, R., & Siame, L. (2012). Deglaciation pattern during the Lateglacial/Holocene transition in the southern French Alps. Chronological data and geographical reconstruction from the Clarée Valley (upper Durance catchment, southeastern France). *Palaeogeography, Palaeoclimatology, Palaeoecology, 315–316*, 109–123. https://doi.org/10.1016/j.palaeo.2011.11.017

Daxer, C. (2020) Topographic Openness Maps and Red Relief Image Maps in QGIS Lacustrine paleoseismology in Carinthia (Austria) and improved seismic intensity assessment based on lake sediments View project Beyond Lake Villages View project, (February). https://doi.org/10.13140/RG.2.2.18958.31047.

Dieleman, C., Ivy-Ochs, S., Hippe, K., Kronig, O., Kober, F., & Christl, M. (2018). Reconsidering the origin of the Sedrun fans (Graubünden, Switzerland). *E&G Quaternary Science Journal, 67*(1), 17–23. https://doi.org/10.5194/egqsj-67-17-2018

Dortch, J. M., Tomkins, M. D., Saha, S., Murari, M. K., Schoenbohm, L. M., & Curl, D. (2022). A tool for the ages: The Probabilistic Cosmogenic Age Analysis Tool (P-CAAT). *Quaternary Geochronology, 71*, Article 101323. https://doi.org/10.1016/j.quageo.2022.101323

Dunai, T. J. (2010). *Cosmogenic nuclides principles, concepts and applications in the earth surface sciences*. Cambridge University Press.

Dunne, J., Elmore, D., & Muzikar, P. (1999). Scaling factors for the rates of production of cosmogenic nuclides for geometric shielding and attenuation at depth on sloped surfaces. *Geomorphology, 27*(1–2), 3–11. https://doi.org/10.1016/S0169-555X(98)00086-5

Federici, P. R., Granger, D. E., Pappalardo, M., Ribolini, A., Spagnolo, M., & Cyr, A. J. (2008). Exposure age dating and Equilibrium Line Altitude reconstruction of an Egesen moraine in the Maritime Alps. *Italy. Boreas, 37*(2), 245–253. https://doi.org/10.1111/j.1502-3885.2007.00018.x

Federici, P. R., Ribolini, A., & Spagnolo, M. (2017). Glacial history of the Maritime Alps from the Last Glacial Maximum to the Little Ice Age. *Geological Society, London, Special Publications, 433*(1), 137–159. https://doi.org/10.1144/SP433.9

Fordham, D. A., Saltré, F., Haythorne, S., Wigley, T. M. L., Otto-Bliesner, B. L., Chan, K. C., & Brook, B. W. (2017). PaleoView: A tool for generating continuous climate projections spanning the last 21 000 years at regional and global scales. *Ecography, 40*(11), 1348–1358. https://doi.org/10.1111/ecog.03031

Furlanetto, G., Ravazzi, C., Badino, F., Brunetti, M., Champvillair, E., & Maggi, V. (2019). Elevational transects of modern pollen samples: Site-specific temperatures as a tool for palaeoclimate reconstructions in the Alps. *The Holocene, 29*(2), 271–286. https://doi.org/10.1177/0959683618810395

Gosse, J. C., & Phillips, F. M. (2001). Terrestrial in situ cosmogenic nuclides: Theory and application. *Quaternary Science Reviews, 20*(14), 1475–1560.

Gross, G., Kerschner, H., & Patzelt, G. (1978). Methodische Untersuchungen über die Schneegrenze in alpinen Gletschergebieten. *Zeitschrift Für Gletscherkunde und Glazialgeologie, 12*, 223–251.

Heiri, O., Koinig, K. A., Spötl, C., Barrett, S., Brauer, A., Drescher-Schneider, R., Gaar, D., Ivy-Ochs, S., Kerschner, H., Luetscher, M., Moran, A., Nicolussi, K., Preusser, F., Schmidt, R., Schoeneich, P., Schwörer, C., Sprafke, T., Terhorst, B., & Tinner, W. (2014). Palaeoclimate records 60–8 ka in the Austrian and Swiss Alps and their forelands. *Quaternary Science Reviews, 106*, 186–205. https://doi.org/10.1016/j.quascirev.2014.05.021

Hepp, J., Wüthrich, L., Bromm, T., Bliedtner, M., Schäfer, I. K., Glaser, B., Rozanski, K., Sirocko, F., Zech, R., & Zech, M. (2019). How dry was the Younger Dryas? Evidence from a coupled δ2H–δ18O biomarker paleohygrometer applied to the Gemündener Maar sediments, Western Eifel. *Germany. Clim. past, 15*(2), 713–733. https://doi.org/10.5194/cp-15-713-2019

Hofmann, F. M., Alexanderson, H., Schoeneich, P., Mertes, J. R., & Léanni, L. (2019). Post-Last Glacial Maximum glacier fluctuations in the southern Écrins massif (westernmost Alps): Insights from 10Be cosmic ray exposure dating. *Boreas, 48*(4), 1019–1041. https://doi.org/10.1111/bor.12405

Isarin, R. F. B., & Renssen, H. (1999). Reconstructing and modelling Late Weichselian climates: The Younger Dryas in Europe as a case study. *Earth-Science Reviews, 48*(1), 1–38. https://doi.org/10.1016/S0012-8252(99)00047-1

Ivy-Ochs, S. (2015). Glacier variations in the European Alps at the end of the last glaciation. *Cuadernos De Investigación Geográfica, 41*(2), 295–315. https://doi.org/10.18172/cig.2750

Ivy-Ochs, S., & Kober, F. (2008). Surface Exposure Dating with Cosmogenic Nuclides. *Quaternary Science Journal (Eiszeitalter und Gegenwart), 57*(1/2), 179–209.

Ivy-Ochs, S., Kerschner, H., & Schlüchter, C. (2007). Cosmogenic nuclides and the dating of Lateglacial and Early Holocene glacier variations: The Alpine perspective. *Quaternary International, 164–65*, 53–63. https://doi.org/10.1016/j.quaint.2006.12.008

Ivy-Ochs, S., Kerschner, H., Maisch, M., Christl, M., Kubik, P. W., & Schlüchter, C. (2009). Latest Pleistocene and Holocene glacier variations in the European Alps. *Quaternary Science Reviews, 28*(21), 2137–2149. https://doi.org/10.1016/j.quascirev.2009.03.009

Ivy-Ochs, S., Kerschner, H., Reuther, A., Maisch, M., Sailer, R., Schaefer, J., Kubik, P. W., Synal, H., & Schlüchter, C. (2006). The timing of glacier advances in the northern European Alps based on surface exposure dating with cosmogenic 10Be, 26Al, 36Cl, and 21Ne. In L. L. Siame, D. L. Bourlès, & E. T. Brown (Eds.), *Application of cosmogenic nuclides to the study of Earth surface processes: The practice and the potential* (Vol. Geological Society of America Special Paper 415, pp. 43–60). Geological Society of America. https://doi.org/10.1130/2006.2415(04)

Ivy-Ochs, S., Monegato, G., & Reitner, J. M. (2023). Chapter 55 - The Alps: glacial landforms from the Younger Dryas Stadial. In D. Palacios, P. D. Hughes, J. M. García-Ruiz, & N. Andrés (Eds.), *European Glacial Landscapes* (pp. 525–539). Elsevier. https://doi.org/10.1016/B978-0-323-91899-2.00058-9.

Ivy-Ochs, S., Schlüchter, C., Kubik, P. W., Synal, H. A., Beer, J., & Kerschner, H. (1996). The exposure age of an Egesen moraine at Julier Pass, Switzerland, measured with the cosmogenic radionuclides 10Be, 26A1 and 36Cl. *Eclogae Geologicae Helvetiae, 89*, 1049–1063.

James, W. H. M., Carrivick, J. L., Quincey, D. J., & Glasser, N. F. (2019). A geomorphology based reconstruction of ice volume distribution at the Last Glacial Maximum across the Southern Alps of New Zealand. *Quaternary Science Reviews, 219*, 20–35. https://doi.org/10.1016/j.quascirev.2019.06.035

Jouvet, G., Cohen, D., Russo, E., Buzan, J., Raible, C. C., Haeberli, W., Kamleitner, S., Ivy-Ochs, S., Imhof, M. A., Becker, J. K., et al. (2023). Coupled climate-glacier modelling of the last glaciation in the Alps. *Journal of Glaciology, 69*(278), 1956–1970.

Jouvet, G., Seguinot, J., Ivy-Ochs, S., & Funk, M. (2017). Modelling the diversion of erratic boulders by the Valais Glacier during the last glacial maximum. *Journal of Glaciology, 63*(239), 487–498.

Karger, D. N., Conrad, O., Böhner, J., Kawohl, T., Kreft, H., Soria-Auza, R. W., Zimmermann, N. E., Linder, H. P., & Kessler, M. (2017). Climatologies at high resolution for the earth's land surface areas. *Scientific Data, 4*(1), Article 170122. https://doi.org/10.1038/sdata.2017.122

Kelly, M. A., Kubik, P. W., Von Blanckenburg, F., & Schluchter, C. (2004). Surface exposure dating of the Great Aletsch Glacier Egesen moraine system, western Swiss Alps, using the cosmogenic nuclide Be-10. *Journal of Quaternary Science, 19*(5), 431–441. https://doi.org/10.1002/jqs.854

Kerschner, H. (2005). Glacier-Climate Models as Palaeoclimatic Information Sources: Examples from the Alpine Younger Dryas Period. In U. M. Huber, H. K. M. Bugmann, spsampsps M. A. Reasoner (Eds.), *Global Change and Mountain Regions: An Overview of Current Knowledge* (pp. 73–81). Springer Netherlands. https://doi.org/10.1007/1-4020-3508-X_8

Kerschner, H., & Ivy-Ochs, S. (2008). Palaeoclimate from glaciers: Examples from the Eastern Alps during the Alpine Lateglacial and early Holocene. *Global and Planetary Change, 60*(1–2), 58–71. https://doi.org/10.1016/j.gloplacha.2006.07.034

Kerschner, H., Kaser, G., & Sailer, R. (2000). Alpine Younger Dryas glaciers as palaeo-precipitation gauges. *Annals of Glaciology, 31*, 80–84. https://doi.org/10.3189/172756400781820237

Kim, C., & Ma, J. (2023). Assessing the Touristic Value of the Stone Run at Mt. *Okryon in the Korean Peninsula. Geoheritage, 15*(2), 65. https://doi.org/10.1007/s12371-023-00841-w

Kohl, C. P., & Nishiizumi, K. (1992). Chemical Isolation of Quartz for Measurement of Insitu-Produced Cosmogenic Nuclides. *Geochimica Et Cosmochimica Acta, 56*(9), 3583–3587.

Korschinek, G., Bergmaier, A., Faestermann, T., Gerstmann, U. C., Knie, K., Rugel, G., Wallner, A., Dillmann, I., Dollinger, G., von Gostomski, C. L., Kossert, K., Maiti, M., Poutivtsev, M., & Remmert, A. (2010). A new value for the half-life of Be-10 by Heavy-Ion Elastic Recoil Detection and liquid scintillation counting. *Nuclear Instruments & Methods in Physics Research Section B-Beam Interactions with Materials and Atoms, 268*(2), 187–191. https://doi.org/10.1016/j.nimb.2009.09.020

Lal, D. (1991). Cosmic-Ray Labeling Of Erosion Surfaces - Insitu Nuclide Production-Rates And Erosion Models. *Earth and Planetary Science Letters, 104*(2–4), 424–439.

Larocque, I., & Finsinger, W. (2008). Late-glacial chironomid-based temperature reconstructions for Lago Piccolo di Avigliana in the southwestern Alps (Italy). *Palaeogeography, Palaeoclimatology, Palaeoecology, 257*(1), 207–223. https://doi.org/10.1016/j.palaeo.2007.10.021

Le Roy, M., Ivy-Ochs, S., Nicolussi, K., Monegato, G., Reitner, J. M., Colucci, R. R., Ribolini, A., Spagnolo, M., & Stoffel, M. (2024). Chapter 20 - Holocene glacier variations in the Alps. In D. Palacios, P. D. Hughes, V. Jomelli, & L. M. Tanarro (Eds.), *European Glacial Landscapes* (pp. 367–418). Elsevier. https://doi.org/10.1016/b978-0-323-99712-6.00018-0

Leger, T. P. M., Jouvet, G., Kamleitner, S., Mey, J., Herman, F., Finley, B. D., Ivy-Ochs, S., Vieli, A., Henz, A., & Nussbaumer, S. U. (2025). A data-consistent model of the last glaciation in the Alps achieved with physics-driven AI. *Nature Communications, 16*(1), 848.

Linsbauer, A., Huss, M., Hodel, E., Bauder, A., Fischer, M., Weidmann, Y., Bärtschi, H., & Schmassmann, E. (2021). The New Swiss Glacier Inventory SGI2016: From a Topographical to a Glaciological Dataset [Original Research]. *Frontiers in Earth Science, Volume 9 - 2021*. https://doi.org/10.3389/feart.2021.704189.

Lotter, A. F., Birks, H. J. B., Eicher, U., Hofmann, W., Schwander, J., & Wick, L. (2000). Younger Dryas and Allerød summer temperatures at Gerzensee (Switzerland) inferred from fossil pollen and cladoceran assemblages.

Palaeogeography, Palaeoclimatology, Palaeoecology, 159(3), 349–361. https://doi.org/10.1016/S0031-0182(00)00093-6
Lukas, S., Graf, A., Coray, S., & Schluchter, C. (2012). Genesis, stability and preservation potential of large lateral moraines of Alpine valley glaciers - towards a unifying theory based on Findelengletscher, Switzerland. *Quaternary Science Reviews, 38*, 27–48. https://doi.org/10.1016/j.quascirev.2012.01.022
Magny, M., Guiot, J., & Schoellammer, P. (2001). Quantitative Reconstruction of Younger Dryas to Mid-Holocene Paleoclimates at Le Locle, Swiss Jura, Using Pollen and Lake-Level Data. *Quaternary Research, 56*(2), 170–180. https://doi.org/10.1006/qres.2001.2257
Marazzi, S. (2005) 'Atlante Orografico delle Alpi. SOIUSA', *Priuli & Verlucca*, p. 416.
Maxeiner, S., Synal, H.-A., Christl, M., Suter, M., Müller, A., & Vockenhuber, C. (2019). Proof-of-principle of a compact 300 kV multi-isotope AMS facility. *Nuclear Instruments and Methods in Physics Research Section B: Beam Interactions with Materials and Atoms, 439*, 84–89. https://doi.org/10.1016/j.nimb.2018.11.028
Meyer (2017): Gesteine der Schweiz, der Feldführer. Bern, Schweiz: Haupt Verlag.
Moran, A. P., Ivy-Ochs, S., Schuh, M., Christl, M., & Kerschner, H. (2016). Evidence of central Alpine glacier advances during the Younger Dryas–early Holocene transition period. *Boreas, 45*(3), 398–410. https://doi.org/10.1111/bor.12170
Müller, F., Caflisch, T., & Müller, G. (1976). Firn und Eis der Schweizer Alpen (Gletscherinventar). Publ. Nr. 57/57a. Geographisches Institut, ETH Zürich, 2 Vols.
Oerlemans, J. (2005). Extracting a climate signal from 169 glacier records. *Science, 308*(5722), 675–677. https://doi.org/10.1126/science.1107046
Ohmura, A., & Boettcher, M. (2018). Climate on the equilibrium line altitudes of glaciers: Theoretical background behind Ahlmann's P/T diagram. *Journal of Glaciology, 64*(245), 489–505. https://doi.org/10.1017/jog.2018.41
Ohmura, A., Kasser, P., & Funk, M. (1992). Climate at the Equilibrium Line of Glaciers. *Journal of Glaciology, 38*(130), 397–411. https://doi.org/10.1017/S0022143000002276
Pellitero, R., Rea, B. R., Spagnolo, M., Bakke, J., Hughes, P., Ivy-Ochs, S., Lukas, S., & Ribolini, A. (2015). A GIS tool for automatic calculation of glacier equilibrium-line altitudes. *Computers & Geosciences, 82*, 55–62. https://doi.org/10.1016/j.cageo.2015.05.005
Pellitero, R., Rea, B. R., Spagnolo, M., Bakke, J., Ivy-Ochs, S., Frew, C. R., Hughes, P., Ribolini, A., Lukas, S., & Renssen, H. (2016). GlaRe, a GIS tool to reconstruct the 3D surface of palaeoglaciers. *Computers & Geosciences, 94*, 77–85. https://doi.org/10.1016/j.cageo.2016.06.008
Pini, R., Furlanetto, G., Vallé, F., Badino, F., Wick, L., Anselmetti, F. S., Bertuletti, P., Fusi, N., Morlock, M. A., Delmonte, B., Harrison, S. P., Maggi, V., & Ravazzi, C. (2022). Linking North Atlantic and Alpine Last Glacial Maximum climates via a high-resolution pollen-based subarctic forest steppe record. *Quaternary Science Reviews, 294*, Article 107759. https://doi.org/10.1016/j.quascirev.2022.107759
Porter, S. C. (1975). Equilibrium-Line Altitudes of Late Quaternary Glaciers in Southern Alps. *New-Zealand. Quaternary Research, 5*(1), 27–47. https://doi.org/10.1016/0033-5894(75)90047-2
Protin, M., Schimmelpfennig, I., Mugnier, J.-L., Ravanel, L., Le Roy, M., Deline, P., Favier, V., Buoncristiani, J.-F., Aumaître, G., Bourlès, D. L., & Keddadouche, K. (2019). Climatic reconstruction for the Younger Dryas/Early Holocene transition and the Little Ice Age based on paleo-extents of Argentière glacier (French Alps). *Quaternary Science Reviews, 221*, Article 105863. https://doi.org/10.1016/j.quascirev.2019.105863
Putkonen, J., & Swanson, T. (2003). Accuracy of cosmogenic ages for moraines. *Quaternary Research, 59*(2), 255–261. https://doi.org/10.1016/S0033-5894(03)00006-1
Rasmussen, S. O., Andersen, K. K., Svensson, A. M., Steffensen, J. P., Vinther, B. M., Clausen, H. B., Siggaard-Andersen, M. L., Johnsen, S. J., Larsen, L. B., Dahl-Jensen, D., Bigler, M., Rothlisberger, R., Fischer, H., Goto-Azuma, K., Hansson, M. E., & Ruth, U. (2006). A new Greenland ice core chronology for the last glacial termination. *Journal Of Geophysical Research-Atmospheres*, *111*(D6). https://doi.org/10.1029/2005JD006079
Rasmussen, S. O., Bigler, M., Blockley, S. P., Blunier, T., Buchardt, S. L., Clausen, H. B., Cvijanovic, I., Dahl-Jensen, D., Johnsen, S. J., Fischer, H., Gkinis, V., Guillevic, M., Hoek, W. Z., Lowe, J. J., Pedro, J. B., Popp, T., Seierstad, I. K., Steffensen, J. P., Svensson, A. M., & Winstrup, M. (2014). A stratigraphic framework for abrupt climatic changes during the Last Glacial period based on three synchronized Greenland ice-core records: Refining and extending the INTIMATE event stratigraphy. *Quaternary Science Reviews, 106*, 14–28. https://doi.org/10.1016/j.quascirev.2014.09.007
Rea, B. R., Pellitero, R., Spagnolo, M., Hughes, P., Ivy-Ochs, S., Renssen, H., Ribolini, A., Bakke, J., Lukas, S., & Braithwaite, R. J. (2020). Atmospheric circulation over Europe during the Younger Dryas. *Science Advances*, *6*(50), eaba4844. https://doi.org/10.1126/sciadv.aba4844
Reitner, J. M., Ivy-Ochs, S., Drescher-Schneider, R., Hajdas, I., & Linner, M. (2016). Reconsidering the current stratigraphy of the Alpine Lateglacial: Implications of the sedimentary and morphological record of the Lienz area (Tyrol/Austria). *E&G Quaternary Sci. J., 65*(2), 113–144. https://doi.org/10.3285/eg.65.2.02
Renssen, H., Goosse, H., Roche, D. M., & Seppä, H. (2018). The global hydroclimate response during the Younger Dryas event. *Quaternary Science Reviews, 193*, 84–97. https://doi.org/10.1016/j.quascirev.2018.05.033
Röthlisberger, F. (1976). Gletscher-und Klimaschwankungen im Raume Zermatt. *Ferpècle und Arolla. Die Alpen, 52*(3–4), 1–152.
Schimmelpfennig, I., Schaefer, J. M., Akcar, N., Koffman, T., Ivy-Ochs, S., Schwartz, R., Finkel, R. C., Zimmerman, S., & Schluchter, C. (2014). A chronology of Holocene and Little Ice Age glacier culminations of the Steingletscher, Central Alps, Switzerland, based on high-sensitivity beryllium-10 moraine dating. *Earth and Planetary Science Letters, 393*, 220–230. https://doi.org/10.1016/j.epsl.2014.02.046
Schindelwig, I., Akçar, N., Kubik, P. W., & Schlüchter, C. (2012). Lateglacial and early Holocene dynamics of adjacent valley glaciers in the Western Swiss Alps. *Journal of Quaternary Science, 27*(1), 114–124. https://doi.org/10.1002/jqs.1523
Schneebeli, W. (1976). Untersuchungen von Gletscherschwankungen im Val de Bagnes: Ein Beitrag zur Rekonstruktion der Klimageschichte des Postglazials. *Die Alpen, 52*, 5–57.
Schneeberger, R., Kober, F., Spillmann, T., Blechschmidt, I., Lanyon, G. W., & Mäder, U. K. (2019). Grimsel Test Site: revisiting the site-specific geoscientific knowledge. Available at: www.nagra.ch
Schwander, J., Eicher, U., & Ammann, B. (2000). Oxygen isotopes of lake marl at Gerzensee and Leysin (Switzerland), covering the Younger Dryas and two minor oscillations, and their correlation to the GRIP ice core. *Palaeogeography, Palaeoclimatology, Palaeoecology, 159*(3), 203–214. https://doi.org/10.1016/S0031-0182(00)00085-7
Scotti, R., Brardinoni, F., Crosta, G. B., Cola, G., & Mair, V. (2017). Time constraints for post-LGM landscape response to deglaciation in Val Viola, Central Italian Alps. *Quaternary Science Reviews, 177*, 10–33. https://doi.org/10.1016/j.quascirev.2017.10.011
Seguinot, J., Ivy-Ochs, S., Jouvet, G., Huss, M., Funk, M., & Preusser, F. (2018). Modelling last glacial cycle ice dynamics in the Alps. *The Cryosphere, 12*(10), 3265–3285.
Spagnolo, M., & Ribolini, A. (2019). Glacier extent and climate in the Maritime Alps during the Younger Dryas. *Palaeogeography, Palaeoclimatology, Palaeoecology, 536*, Article 109400. https://doi.org/10.1016/j.palaeo.2019.109400
Steck, A. (2011) 'Blatt 1269 Aletschgletscher', *Geologischer Atlas der Schweiz 1/25 000. Erläuterungen*, p. 68.
Stone, J. O. (2000). Air pressure and cosmogenic isotope production. *Journal of Geophysical Research-Solid Earth, 105*(B10), 23753–23759.
Tektonische Karte der Schweiz, 1:500000. Geologische Bearbeitung durch Institut für Geologie der Universität Bern und durch Bundesamt für Wasser und Geologie, 2005, ISBN 3–906723–56–9.
Tikhomirov, D., Akçar, N., Ivy-Ochs, S., Alfimov, V., & Schluchter, C. (2014). Calculation of shielding factors for production of cosmogenic nuclides in fault scarps. *Quaternary Geochronology, 19*, 181–193. https://doi.org/10.1016/j.quageo.2013.08.004
Tinner, W., & Theurillat, J.-P. (2003). Uppermost Limit, Extent, and Fluctuations of the Timberline and Treeline Ecocline in the Swiss Central Alps during the Past 11,500 Years. *Arctic, Antarctic, and Alpine Research, 35*(2), 158–169. https://doi.org/10.1657/1523-0430(2003)035[0158:ULEAFO]2.0.CO;2
von Raumer, J. F., Ménot, R. P., Abrecht, J., spsampsps Biino, G. (1993). The Pre-Alpine Evolution of the External Massifs. In J. F. von Raumer spsampsps F. Neubauer (Eds.), *Pre-Mesozoic Geology in the Alps* (pp. 221–240). Springer Berlin Heidelberg. https://doi.org/10.1007/978-3-642-84640-3_13

Winkler, S. (2009). *Gletscher und ihre Landschaften*. Wissenschaftliche Buchgesellschaft.
Ye, S., Cuzzone, J. K., Marcott, S. A., Licciardi, J. M., Ward, D. J., Heyman, J., & Quinn, D. P. (2023). A quantitative assessment of snow shielding effects on surface exposure dating from a western North American 10Be data compilation. *Quaternary Geochronology, 76*, Article 101440. https://doi.org/10.1016/j.quageo.2023.101440

Publisher's Note